Optimal and regulated transcription facilitates formation of damage-induced cohesion

Pei-Shang Wu[1], Donald P. Cameron[1 ‡], Jan Grosser[1‡], Laura Baranello[1] and Lena Ström[1*]

[1] Karolinska Institutet, Department of Cell and Molecular Biology, SE-171 77 Stockholm, Sweden

Running title: Transcription facilitates DI-cohesion

‡ These authors contributed equally to this work

* Corresponding Author: Lena Ström, Karolinska Institutet, Department of Cell and Molecular Biology, Biomedicum, B07, +46-8-524 870 43, lena.strom@ki.se

Total character count: 57 455 (including spaces, excluding references)

Abstract

The SMC complex cohesin mediates sister chromatid cohesion established during replication, and damage-induced cohesion formed in response to DSBs post replication. The translesion synthesis polymerase Polη is required for damage-induced cohesion through a hitherto unknown mechanism. Since Polη is functionally associated with transcription, and transcription triggers *de novo* cohesion in *S. pombe*, we hypothesized that active transcription facilitates damage-induced cohesion in *S. cerevisiae*. Here, we found that expression of genes involved in chromatin assembly and positive transcription regulation were relatively enriched in WT compared to Polη-deficient cells (*rad30Δ*). The *rad30Δ* mutant showed a dysregulated transcriptional response and increased cohesin binding around transcription start sites. Perturbing histone exchange at promoters adversely affected damage-induced cohesion, similarly to deletion of *RAD30*. Conversely, altering chromatin accessibility or regulation of transcription elongation, suppressed the lack of damage-induced cohesion in *rad30Δ* cells. These results indicate that Polη promotes damage-induced cohesion through its role in transcription, and support the model that regulated transcription facilitates formation of damage-induced cohesion.

Keywords: Cohesin/ Damage-induced cohesion/ nucleosome dynamics/ Polymerase eta/ transcription

Introduction

Dynamic disassembly and reassembly of nucleosomes, the building blocks of chromatin, facilitates processes such as replication and transcription. During the course of chromatin assembly, the nucleosomal histones are exchanged with histone variants or post-translationally modified histones. This affects physical and chemical properties of nucleosomes, as well as chromatin accessibility. Replication-independent nucleosome assembly, or so-called histone exchange, aids and regulates RNA polymerase II (RNAPII) passage through the nucleosomes during transcription initiation and elongation (Terweij & van Leeuwen, 2013). This is accomplished through histone chaperones, in concert with histone modifying enzymes and chromatin remodelers (Venkatesh & Workman, 2015).

Transcription is not only the instrument for gene expression, but is also connected to cohesin localization on chromosomes. Cohesin is one of the structural maintenance of chromosomes (SMC) protein complexes, with the core formed by Smc1, Smc3 and the kleisin Scc1. Cohesin dynamically associates with chromosomes at intergenic regions of convergent genes, possibly as a result of active transcription (Bausch et al, 2007; Lengronne et al, 2004). Cohesin and its loader Scc2 have been implicated in gene regulation (Dorsett & Strom, 2012; Lopez-Serra et al, 2014). These proteins also spatially organize chromosomes into topologically associated domains (TADs), through DNA loop extrusion (Davidson et al, 2019; Haarhuis et al, 2017; Kim et al, 2019b; Lazar-Stefanita et al, 2017; Schalbetter et al, 2017). Interestingly, formation of cohesin dependent TAD-like structures is partly mediated by the histone chaperone FACT (Facilitates chromatin transactions) complex in *S. cerevisiae* (Garcia-Luis et al, 2019), suggesting a connection between chromosome organization and chromatin assembly.

In addition to the roles described above, the canonical role of cohesin is to mediate sister chromatid cohesion. Cohesin is recruited to chromatin by the cohesin loading complex Scc2-Scc4 from late G_1 phase in *S. cerevisiae* (Ciosk et al, 2000). Loading of cohesin continues through the cell cycle, both dependently and independently of Scc2-Scc4 (Srinivasan et al, 2020). During S-phase, cohesin becomes cohesive through acetylation of Smc3 by the acetyltransferase Eco1 (Rolef Ben-Shahar et al, 2008; Unal et al, 2008; Zhang et al, 2008a). The established sister chromatid cohesion is then maintained until anaphase (Uhlmann et al, 1999), ensuring faithful chromosome segregation.

At the end of S phase, Eco1 is targeted for degradation. However, inducing a single site-specific double strand break post-replication (G_2/M) is sufficient to stabilize Eco1 (Lyons et al, 2013; Lyons & Morgan, 2011). Presence of active Eco1 then allows generation of damage-induced cohesion in G_2/M, which is established close to the break, and also genome wide on undamaged chromosomes (Strom et al, 2007; Strom et al, 2004; Unal et al, 2007). We previously showed that Polymerase eta (Polη), one of three translesion synthesis (TLS) polymerases in *S. cerevisiae*, is specifically required for genome wide damage-induced cohesion (Enervald et al, 2013).

Polη (encoded by the *RAD30* gene) is well characterized for bypassing bulky lesions induced by ultraviolet irradiation (Johnson et al, 1999), yet emerging evidence suggest that Polη also exhibits TLS-independent functions (Acharya et al, 2019). Polη is the only TLS polymerase required for damage-induced cohesion (Enervald et al, 2013), independently of its polymerase activity, but dependent on Polη-S14 phosphorylation; potentially mediated by the cyclin dependent kinase, Cdc28 (Wu et al, 2020). However, the underlying role of Polη in damage-induced cohesion remains

unclear. Thus, absence of Polη does not affect break-proximal damage-induced cohesion or DSB repair. Lack of Polη also does not perturb Eco1 stabilization, cohesin chromatin association or Smc3 acetylation after DSBs in G_2/M (Enervald et al, 2013).

Based on the following two observations we hypothesized that active transcription facilitates damage-induced cohesion genome wide. First, Polη is enriched at actively transcribed regions, and required for expression of several active genes in *S. cerevisiae* (Gali et al, 2017). Second, activated transcription leads to establishment of local *de novo* cohesion in *S. pombe* (Bhardwaj et al, 2016). Here, we present data pointing at a role for Polη and Polη-S14 phosphorylation in facilitating chromatin association of RNAPII. In addition, the transcriptional program in the Polη null mutant (*rad30Δ*) is altered both before and after DSB induction, compared to WT cells. In WT cells genes involved in chromatin assembly and positive transcription regulation were relatively enriched compared to the *rad30Δ* mutant. Perturbing histone exchange at promoter regions by a *HIR1* or *HTZ1* deletion negatively affects damage-induced cohesion formation, in a similar fashion as in *rad30Δ* cells. Deletion of the DNA architectural protein Nhp6, or the transcription elongation regulator Set2 however, suppress the lack of damage-induced cohesion in the *rad30Δ* mutant. Taken together, our results indicate that Polη is required for damage-induced cohesion through its role in transcription, and support the model that regulated transcription facilitates formation of damage-induced cohesion.

Results

A potential role for Polη in facilitating chromatin association of RNAPII

To test if active transcription is correlated with generation of damage-induced cohesion, we began by determining sensitivity of the damage-induced cohesion deficient *rad30Δ* and *Polη-S14A* cells to inhibition of transcription elongation. Indeed, viability of the mutants decreased when exposed to actinomycin D (Fig 1A). Consistent with a previous report (Gali et al, 2017), *rad30Δ* cells were also sensitive to mycophenolic acid (MPA). This sensitivity was reversed by supplementing guanine in the media (Fig 1A), verifying that it was due to depletion of the guanylic nucleotide pool (Desmoucelles et al, 2002). The *Polη-S14A* point mutant was similarly sensitive to MPA as the null mutant (Fig 1A). Sensitivity to elongation inhibitors could be due to reduced transcriptional capacity. We therefore monitored chromatin association of Rpb1, the largest subunit of RNAPII, in these mutants. Binding of Rpb1 at promoters and coding regions of selected active genes was reduced in both *rad30Δ* and *Polη-S14A* mutants compared to WT cells (Fig 1B). The reduced chromatin association was accompanied with increased level of total Rpb1 in the null and *Polη-S14A* mutants (Fig 1C, Appendix Fig 1A). Furthermore, Rpb1 in these mutants was as stable as that in the WT cells, regardless of DSB induction (Fig 1C and D, Appendix Fig 1A and B). Here and throughout the study the DSBs were induced at the *MAT* locus on chromosome III (P_{GAL}-*HO*) for one-hour, unless otherwise stated. These results together suggest that Polη facilitates chromatin association of RNAPII for proper transcription initiation and elongation, independent of DNA damage, possibly through phosphorylation of Polη-S14.

Transcription is perturbed in *rad30Δ* mutants

To further pinpoint a potential connection between transcription and formation of damage-induced cohesion, we focused on the *rad30Δ* mutant for the following investigations. To begin with, we analyzed gene expression of G_2/M arrested WT and *rad30Δ* cells, before and after one-hour break induction, by RNA-sequencing analysis (RNA-seq). Prior to RNA-seq, G_2/M arrest and break induction were confirmed (Fig EV1A and B). Principal component analysis (PCA) showed that the individual data sets were distributed as distinct clusters (Fig EV1C). Differences in gene expression patterns between WT and *rad30Δ* cells were readily observed before break induction, with 395 genes upregulated and 439 genes downregulated in the G_2/M arrested *rad30Δ* mutant (Fig 2A). As compared to the WT cells which showed 473 genes up- and 519 genes down-regulated after DSB induction (Fig 2B), there were 360 and 230 genes up- and down-regulated respectively in the *rad30Δ* mutant (Fig 2C, Dataset EV1). While the differentially expressed genes in WT and *rad30Δ* cells after break induction significantly overlapped (Fig EV1D) and trended in the same direction, the up- and down-regulation after DSB was of greater magnitude in the WT cells (Fig 2D and E). This implied that the response to break induction in the *rad30Δ* cells is similar, but relatively attenuated in comparison to the WT cells' response. Furthermore, we noted that short genes tended to be upregulated compared to long genes in WT cells after DSB induction (Fig 2F), similar to the reported gene length dependent changes of expression after UV exposure (McKay et al, 2004; Williamson et al, 2017). In contrast, differential expression after DSBs is independent of gene length in the *rad30Δ* mutant (Fig 2F). These results clearly show that *RAD30* deletion leads to transcription deregulation, both in unperturbed G_2/M phase and in response to break induction.

Increased cohesin binding around TSS in *rad30Δ* cells

SInce transcription is deregulated in the *rad30Δ* mutant, and active transcription results in cohesin localization at the ends of convergent genes (Lengronne A 2004, Bausch C 2007), we asked if cohesin distribution is affected at gene units in *rad30Δ* compared to WT cells. To address this question, we revisited our previous Scc1 ChIP-sequencing data (GSE42655), from which we concluded that cohesin binding was similar with and without break induction in the WT cells, except at the break site. Also, absence of Polη did not result in apparent differences in overall cohesin binding (Enervald et al, 2013). The upregulation of short genes in WT cells after DSBs (Fig 2F), also appeared to be independent of cohesin binding (Fig EV1E). From these results, transcription responses do not seem to directly correlate with cohesin distribution in G_2/M phase. However, when focusing on cohesin binding at transcription start site (TSS) and transcription end site (TES), a relatively increased binding around (TSS) was observed in *rad30Δ* compared to WT cells (Fig 3A and B). This increased accumulation was not found around TES (Fig 3C and D), and independent of DSB induction (Fig 3A-D). Since transcription is deregulated in *rad30Δ* cells before and after DSBs, this indicates that transcription dysregulation could still result in a regional difference in cohesin distribution around TSS.

Genes involved in chromatin assembly and positive transcription regulation pathways are downregulated in the absence of Polη

To gain mechanistic insight into the diverse transcriptional responses detected in WT and *rad30Δ* cells, the differentially expressed genes between WT and *rad30Δ* cells (before and after DSBs) were analyzed by Gene Set Enrichment Analysis

(GSEA), followed by generation of enriched pathway maps with Cytoscape as shown in Fig 4. The gene sets under each annotated group are listed in Dataset EV2 and 3. During G_2/M arrest, genes that belong to biological pathways such as chromatin assembly and positive transcription regulation were enriched in WT compared to *rad30Δ* cells (Fig 4A). When comparing gene expression after break induction, the pathways illustrated in Fig 4B were clearly differentially regulated between WT and *rad30Δ* cells. WT cells tended to downregulate essential cell homeostatis pathways, such as ribosome biogenesis and various metabolism pathways, relative to the *rad30Δ* mutant. This further indicates deregulation of gene expression in the *rad30Δ* mutant. However, despite that some genes belonging to the cellular response to DNA damage stimulus pathway (GO: 6974) were upregulated in WT cells, this pathway was overall not significantly enriched. In addition, activation of the DNA damage checkpoint, as indicated by phosphorylation of Rad53, was only observed during the recovery period after DSB induction in WT and *rad30Δ* cells (Fig EV2A and B), with no difference in cell cycle progression between populations (Fig EV2C). These results indicate that the lack of damage-induced cohesion in *rad30Δ* cells is not due to a possible difference in activation of the DNA damage checkpoint. Therefore, we decided to test the potential connection between transcription and damage-induced cohesion, focusing on two of the pathways differentially enriched in the WT cells: Chromatin assembly and positive transcription regulation.

Histone exchange at promoters affects formation of damage-induced cohesion

To test the idea that the deficient damage-induced cohesion in *rad30Δ* cells would be due to transcriptional dysregulation, we set out to mimic or reverse this

situation by deleting candidates of interest, alone or in combination with deletion of the *RAD30* gene.

To this end, we investigated whether Hir1, a component of the HIR complex involved in replication-independent nucleosome assembly (Green et al, 2005; Prochasson et al, 2005), is required for damage-induced cohesion. Histone H3 exchange mediated by the HIR complex and the histone chaperone Asf1 mainly takes place at promoters, correlated with active transcription. However, basal H3 exchange also occurs to poise inactive promoters for optimal transcription (Dion et al, 2007; Rufiange et al, 2007). To monitor damage-induced cohesion, DSBs and ectopic P_{GAL}-*SMC1-MYC* expression were induced by addition of galactose to G_2/M arrested cells. Due to *smc1-259 ts* background, cohesion established during replication was inactivated by a temperature raise. Damage-induced cohesion generated with the ectopic Smc1-Myc was examined with an integrated TetO/TetR-GFP array (illustrated in Appendix Fig 2A). G_2/M arrest, break induction and protein expression of the ectopic Smc1-Myc were confirmed for all experiments, with examples shown in Fig EV3A-C. Interestingly, formation of damage-induced cohesion was partially deficient in the *hir1Δ* mutant, while the *hir1Δrad30Δ* double resembled the *rad30Δ* single mutant, although with slower sister separation (Fig 5A). This indicated that Hir1 and Polη are both required for efficient damage-induced cohesion; possibly acting in the same pathway.

In a similar manner as the basal H3 exchange, incorporation of the H2A variant Htz1 (H2A.Z), preferentially at promoters, allows transcription of otherwise inactive genes (Li et al, 2005; Zhang et al, 2005). Incorporation of Htz1 also relieves the +1 nucleosome barrier to RNAPII (Rhee et al, 2014; Weber et al, 2014). Thus, we monitored damage-induced cohesion formation in an *htz1Δ* mutant. Since it does not

respond to P_{GAL}-*HO* induction (Morillo-Huesca et al, 2010), γ-irradiation was utilized as source of DSB induction (see Appendix supplementary methods). Similar to the *hir1Δ* mutant (Appendix Fig 2B, Fig EV3D), the *htz1Δ* mutant showed impaired damage-induced cohesion (Fig 5B). In contrast to a previous report (Sharma et al, 2013), we did not observe a cohesion maintenance defect due to *HTZ1* deletion (Fig EV3E). These results suggest that perturbing histone exchange at promoters, needed for proper transcriptional response, negatively affects formation of damage-induced cohesion.

Globally reduced nucleosome occupancy does not affect formation of damage-induced cohesion

From the gene sets belonging to the chromatin assembly and positive transcription regulation groups (Fig 4A), we chose to further investigate *NHP6A*. Nhp6 is a high mobility group-B (HMGB) protein that binds and bends DNA (Paull & Johnson, 1995; Yen et al, 1998), but the detailed mechanism of Nhp6 function in transcription remains to be investigated (Kozlova et al, 2018). Deleting the functionally redundant *NHP6A* and *NHP6B* genes (Costigan et al, 1994) however results in reduced nucleosome occupancy especially around TSS and increased transcription (Celona et al, 2011). Therefore, we were interested in knowing if deletion of the *NHP6* genes would rescue the damage-induced cohesion defect of the *rad30Δ* mutant. Since the *nhp6aΔnhp6bΔ* mutant did not respond to P_{GAL}-*HO* induction (Paull et al, 1996; Yu et al, 2000), we monitored damage-induced cohesion after γ-irradiation exposure (Appendix Fig 2B). Generation of damage-induced cohesion was not impaired in the *nhp6aΔnhp6bΔ* mutant. Interestingly, deleting

NHP6A and *NHP6B* indeed rescued the *rad30Δ* mutant from its lack of damage-induced cohesion (Fig 6A, Fig EV4A).

We then tested if globally reduced nucleosome occupancy affects formation of damage-induced cohesion. *HHT1-HHF1* and *HHT2-HHF2* are the two H3-H4 coding gene pairs, where the later contributes to approximately 85% of the total H3-H4 transcripts (Yu et al, 2019). Compared to the WT cells, deletion of either H3-H4 gene pair had no effect on damage-induced cohesion (Fig 6B). Also, unlike the *nhp6aΔnhp6bΔ* mutant, globally reduced nucleosome occupancy by *HHT2-HHF2* deletion (Yu et al, 2019) did not suppress the deficient damage-induced cohesion of the *rad30Δ* mutant (Fig 6C). Because of this, we examined chromatin accessibility of the *nhp6aΔnhp6bΔ* mutant by titrated MNase digestions. In contrast to the previous report where asynchronous cells were analyzed (Celona et al, 2011), we found that the bulk chromatin in G_2/M arrested *nhp6aΔnhp6bΔ* was less accessible than the WT cells, indicating an increase of global nucleosome occupancy (Fig EV4B). Interestingly, compared to WT cells, the *rad30Δ* mutant was slightly more resistant to MNase digestion. In addition, the *nhp6aΔnhp6bΔrad30Δ* mutant showed an intermediate resistance to MNase when compared to *nhp6aΔnhp6bΔ* and *rad30Δ* cells (Fig EV4B). Since globally reduced nucleosome occupancy does not affect formation of damage-induced cohesion, deletion of the *NHP6* genes likely suppresses the lack of damage-induced cohesion in *rad30Δ* cells through an alternative compensatory mechanism based on the altered chromatin accessibility.

A positive role for Polη in transcription is essential for generation of damage-induced cohesion

Another protein that we were interested in testing for damage-induced cohesion was Set2, a histone lysine methyltransferase that regulates transcription initiation (Landry et al, 2003; Strahl et al, 2002) and elongation (Govind et al, 2010; Ruan et al, 2015; Venkatesh et al, 2012). Since Set2 negatively affects transcription initiation (Biswas et al, 2006; Landry et al, 2003; Strahl et al, 2002), while Polη appears to facilitate chromatin association of RNAPII (Fig 1A-D), removal of Set2 in Polη-deficient cells could compensate for the deficient transcription. Therefore, we tested if deletion of *SET2* would suppress the sensitivity of *rad30Δ* cells to transcription elongation inhibitors. The *set2Δ* mutant showed no obvious sensitivity to these inhibitors, especially actinomycin D. Interestingly, deletion of the *SET2* gene masked the sensitivity of the *rad30Δ* mutant to actinomycin D (Fig 7A). Similarly, if Polη is required for damage-induced cohesion through its positive role in transcription, deletion of *SET2* should also suppress deficient damage-induced cohesion of *rad30Δ* cells. We found that the *set2Δ* mutant resembled the WT cells in formation of damage-induced cohesion. Noticeably, deletion of *SET2* indeed suppressed the lack of damage-induced cohesion in the *rad30Δ* mutant (Fig 7B). This clearly suggests that Polη´s positive role in transcription is important for formation of damage-induced cohesion.

Taken together, the results presented here (depicted in Fig 7C) support the idea that an optimal and regulated transcriptional response facilitates formation of damage-induced cohesion. Absence of Polη perturbs transcription regulation, which in turn results in deficient damage-induced cohesion.

Discussion

In this study, we show that Polη-deficient cells display severly altered transcriptional regulation, both in unchallenged G_2/M arrested cells and in response to DSBs. Transcription elongation defeciency was corroborated by increased sensitivity of Polη-deficient cells to transcription elongation inhibitors (Fig 1A). It could be argued that the sensitivity to actinomycin D would be a consequence of DNA damage since actinomycin D also inhibits topoisomerases (Trask & Muller, 1988), leading to formation of DSBs. However, since the *rad30Δ* mutant is insensitive to specific topoisomerase inhibitors, such as camptothecin and etoposide (Bi et al, 2015; Segovia et al, 2017), this is less likely.

Based on our gene set enrichment analysis, mitochondrial related pathways were enhanced in the absence of Polη (Fig 4A-B and Dataset EV2-3). This is an interesting observation since genes involved in the tricarboxylic acid cycle and oxidative phosphorylation were similarly upregulated in mutants with defective chromatin assembly (Galdieri et al, 2016). To test the idea that the lack of damage-induced cohesion in *rad30Δ* cells would be due to transcriptional dysregulation, we began by testing the requirement of HIR/Asf1 mediated histone exchange for damage-induced cohesion, from the perspective of chromatin assembly. By deleting the *HIR1* gene, which is sufficient to disrupt the HIR/Asf1 interaction (Green et al, 2005), we found that the *hir1Δ* mutant is partially deficient in damage-induced cohesion (Fig 5A and EV3D). The role of the HIR complex in damage-induced cohesion might appear difficult to pinpoint since it is involved in multiple processes. Considering the HIR-dependent histone gene repression (Sherwood et al, 1993), the partial deficiency of the *hir1Δ* mutant in damage-induced cohesion could be due to elevated histone gene expression. If so, reducing the histone gene dosage should be beneficial for the *rad30Δ* mutant in generation of damage-induced cohesion.

However, deleting the H3-H4 histone gene pairs did not alter the *rad30Δ* phenotype in damage-induced cohesion formation (Fig 6C). This reversely indicates that the partial deficiency of the *hir1Δ* mutant is not due to altered histone levels. Furthermore, the HIR complex has been implicated in multiple processes, such as formation of a functional kinetochore (Sharp et al, 2002) and heterochromatic gene silencing (Kaufman et al, 1998), which might be important for establishment of damage-induced cohesion. However, the chromatin assembly complex-1 (CAF-1) is redundant with the HIR complex in these processes. Deletion of Hir1 is thereby not likely to perturb other processes than histone exchange. Together, this suggests a direct role for HIR-dependent histone exchange in damage-induced cohesion.

We also tested if deletion of Nhp6 would rescue the *rad30Δ* mutant from lack of damage-induced cohesion (Fig 6A). WT Nhp6a binding is strongly associated with nucleosomes that show altered position and reduced occupancy in transcribed regions (Gossett & Lieb, 2012). In line with this, in the *nhp6aΔnhp6bΔ* mutant the global nucleosome occupancy was inversely increased (Fig EV4B). Nhp6 deletion may suppress the deficient damage-induced cohesion of *rad30Δ* cells by changing chromatin conformation of specific regulatory regions that Nhp6 normally binds to, thereby limiting access of transcription repressors and corepressors to chromatin. This could occur directly through Nhp6, which can modulate chromatin properties on its own (Rhoades et al, 2004), or through protein complexes interacting with Nhp6. The weakly associated FACT complex would be an interesting candidate to study, since this complex mediates cohesin localization and formation of TAD-like structures, independently of sister chromatid cohesion (Garcia-Luis et al, 2019). However, Nhp6 is a prerequisite for the nucleosome association of FACT (Formosa et al, 2001; Xin et al, 2009), suggesting that the observed supression can happen

without the FACT complex. It would also be interesting to test another Nhp6 interactor, the RSC complex (Hepp et al, 2014; Szerlong et al, 2003), but disruption of this complex also affects cohesin chromatin association (Lopez-Serra et al, 2014). The complexes interacting with Nhp6 were therefore not further tested for damage-induced cohesion here.

Since Polη appears to facilitate chromatin association of RNAPII (Fig 1A-D), we tested the effect of removing the transcription regulator Set2 on the *rad30Δ* mutant for formation of damage-induced cohesion. Removal of *SET2* caused an increased RNAPII association towards the 3'-end of actively transcribed genes, indicating active transcription elongation (Kizer et al, 2005). Since the *set2Δ* and *set2Δrad30Δ* mutants are equally insensitive to the tested transcription elongation inhibitors (Fig 7A), deletion of *SET2* might similarly increase chromatin association of RNAPII in the *rad30Δ* mutant. This possibility, together with the increased histone exchange and histone acetylation within coding regions of a *set2Δ* mutant (Venkatesh et al, 2012) could compensate for the reduced transcriptional capacity of *rad30Δ* cells. Importantly, the *SET2* deletion suppresses the lack of damage-induced cohesion in *rad30Δ* cells (Fig 7B). This genetic evidence supports the idea that Polη is involved in damage-induced cohesion through its positive role in transcription.

Polη´s function in transcription was proposed to depend on its polymerase activity (Gali et al, 2017), while its role in damage-induced cohesion was not (Enervald et al, 2013). The finding that transcription facilitates formation of damage-induced cohesion could therefore be seen as conflicting with a polymerase-independent role of Polη in damage-induced cohesion. However, we previously showed that the putative Polη-S14 phosphorylation is required for damage-induced cohesion, but not for cell survival after UV irradiation (Wu et al, 2020), which depends

on Polη polymerase activity. In addition, the *Polη-S14A* mutant exhibits similar elongation inhibitor sensitivity and altered Rpb1 behaviour as the *rad30Δ* mutant (Fig 1A-D). This together indicates that the polymerase activity is not the sole requirement for Polη in transcription, and the detailed mechanism for its function in transcription would clearly be interesting to explore further.

In addition to perturbed transcriptional regulation, increased cohesin binding around TSS was observed in *rad30Δ* cells, independently of DSBs (Fig 2 and 3). This indicates that transcriptional regulation might also modulate the dynamics and/or positioning of cohesin at cohesin associated regions. Since the boundaries of cohesin mediated TAD-like structures often form at promoters of active genes in yeast (Hsieh et al, 2015), a reciprocal interplay between transcription and formation of TAD-like structure has been suggested (van Steensel & Furlong, 2019). It would be interesting to investigate if TAD-like structures are altered in *rad30Δ* cells, in connection with this potential reciprocal interplay.

Through perturbing histone exchange, altering chromatin accessibility and removing a transcription elongation regulator, we show that a regulated transcriptional response potentially facilitates generation of damage-induced cohesion post-replication. Since establishment of sister chromatid cohesion is proposed to occur simultaneously with replication fork progression (Lengronne et al, 2006; Srinivasan et al, 2020) in concert with replication-coupled nucleosome assembly (Zhang et al, 2017), replication-independent nucleosome assembly could be utilized as an alternative platform for generation of damage-induced cohesion after replication. Deregulated transcription in *rad30Δ* cells might perturb progression of this platform, in turn affecting formation of damage-induced cohesion.

Despite the subtle defect in chromosome segregation observed in the *rad30Δ* mutant (Enervald et al, 2013), the importance of genome wide damage-induced cohesion remains to be determined. It might be relevant to the increased chromosome mobility in response to DSBs, which presumably facilitates the search of sequence homology for recombination (Dion et al, 2012; Mine-Hattab & Rothstein, 2012). Interestingly, the movement at the same time is constrained by sister chromatid cohesion (Dion et al, 2013). Since unbroken chromosomes are known to be less mobile than broken chromosomes (Dion et al, 2012; Mine-Hattab & Rothstein, 2012), formation of genome-wide damage-induced cohesion might further limit the movements of undamaged chromosomes, to reduce the chance of unfavorable recombinations.

Materials and methods

Yeast strains and media

All *S. cerevisiae* yeast strains, listed in Table EV1, were W303 derivatives (*ade2-1 trp1-1 can1-100 leu2-3, 112 his3-11, 15 ura3-1 RAD5 GAL psi*$^{+}$). To create null mutants, the gene of interest was replaced with an antibiotic resistance marker through lithium acetate based transformation. Some strains were crossed to obtain desired genotypes. Yeast extract peptone (YEP) supplemented with 40 µg/ml adenine was used as yeast media, unless otherwise stated.

Spot assay

Cell culturing and subsequent serial dilutions were performed as described (Wu et al, 2020). Each dilution was sequentially spotted on uracil drop-out (-Ura) media, containing actinomycin D, MPA, or solvent only (final 1.2% ethanol in plates). Guanine was supplemented at 0.3 mM final concentration (Sagot et al, 2005). The plates were kept at room temperature and documented on the third day. Each spot assay was done at least twice.

Protein extraction and western blotting

Whole cell extracts (WCEs) were prepared with glass bead disruption, TCA or a sodium hydroxide based method (Kushnirov, 2000). To monitor Rpb1 stability, cycloheximide (Sigma) was supplemented in media (final 100µg/ml), and the protein extracts were prepared with sodium hydroxide based method. Bolt 4-12% Bis-Tris or NuPAGE 3-8% Tris-Acetate gels (Invitrogen) were used for electrophoresis, with Bolt MOPS or NuPAGE Tris-Acetate SDS running buffer (Invitrogen). Proteins were transferred to nitrocellulose membranes with the Trans-blot Turbo system (Bio-Rad) or the XCell II Blot Module (Invitrogen). Antibody information is listed in the Appendix Table 1. Odyssey Infrared Imaging and BioRad chemiluminescence system were used for antibodies detections. Image Studio Lite software was used for quantitation of protein bands.

Chromatin immunoprecipitation (ChIP)-qPCR

ChIP was in essence performed as described with some modifications (Enervald et al, 2013). Cells were crosslinked with 1% formaldehyde, for 20 minutes at room temperature, washed three times in 1X cold TBS and mechanically lysed using a

6870 freezer/mill (SPEX, CertiPrep). WCEs were subjected to chromatin shearing by sonication (Bandelin, Sonopuls) for chromatin fragments of 3-500 bp. Anti-Rpb1 was coupled to magnetic dynabeads protein A beads (Invitrogen), and used for immunoprecipitation at 4°C, overnight. Crosslinking of eluted IP and input samples was reversed, and DNA was purified. DNA analysis was performed by real time qPCR using SYBR Green (Applied Biosystems), according to manufacturer's guidelines on an ABI Prism 7000 sequence detection system (Applied Biosystems). The genes of interest were selected based on the RNA-seq results. Primers used are listed in Table EV2. Statistical analysis was performed with SPSS statistics software (IBM).

Total RNA extraction

For RNA-seq, G_2/M arrested cells (about 9 OD_{600}) were harvested before and after 1-hour P_{GAL}-*HO* break induction. Equal amount of samples were additionally collected at each time-point as genomic DNA (gDNA) controls. The gDNA content of each sample was determined prior to total RNA extraction. Total RNA extracts were prepared with PureLink RNA Mini Kit (Invitrogen), with some modifications of the manufacture's guidelines. Collected cell pellets were washed once with SE mix (final 1 M sorbitol and 50 mM EDTA), and resupended with 100 µl zymolyase lysis buffer (SE mix supplemented with final 3 mg/ml 100T zymolyase (Sunrise Science) and 2.5 µl Ribolock (Invitrogen). The suspension was incubated at 30°C for 60 minutes, followed by addition of 200 µl kit-provided RNA lysing buffer, supplemented with Ribolock. The rest of the procedure was performed according to the manufacture's guidelines. To elute total RNA from columns, the volume of RNase free water for

elution was adjusted according to gDNA content of each sample. For each strain, equal volume of the total RNA extract was further purified with DNA-free Kit (Invitrogen).

RNA-sequencing and ChIP-sequencing data analyses

Total RNA samples prepared for RNA-seq (triplicates) were subsequently handled by Novogene for library construction (250-300 bp insert cDNA library) and RNA sequencing (Illumina HiSeq X Ten, paired-end, 10 M reads). Quality controls were included for the total RNA samples and during the procedures for RNA-sequencing.

FASTQC (https://www.bioinformatics.babraham.ac.uk/projects/fastqc/) was used for quality control of the .fastq-files for both RNA- and ChIP-seq. Adapter and poor quality read trimming was performed with cutadapt (Martin, 2011). The RNA-seq data was mapped with the splice-aware aligner HISAT2 (Kim et al, 2019a). The ChIP-seq data was mapped using bowtie (Langmead et al, 2009) with the colorspace option enabled. Afterwards the mapped files were sorted using samtools (Li & Durbin, 2009). Both sets of sequencing data were aligned to the yeast genome version SacCer3 downloaded from UCSC genome browser. Duplicates in the mapped .bam-files were removed using MarkDuplicates (http://broadinstitute.github.io/picard) from the Picard toolset. Deeptools2 (Ramirez et al, 2016) was used to calculate the coverage and to generate bigwig-files.

For the RNA-seq data set, the reads were counted per gene using featureCounts (Liao et al, 2014). The count-files were imported into R and further analyzed using edgeR (McCarthy et al, 2012; Robinson et al, 2010) for FPKM calculations and DESeq2 (Love et al, 2014) for differential expression analysis.

Differential expression analysis yielded fold-changes alongside significance for genes, additionally DESeq2 was used to generate principal component analysis plots. Genes with a total read count below 10 across all samples as well as those producing NAs (not available) in any of the comparisons for fold-change calculation were excluded from the analysis. As all four conditions showed a similar within-group variability in the PCA plot, for all fold-change calculations all samples were run together as opposed to subsetting the samples of interest e.g. WT G2 + DSB vs. WT G2. This allowed for more accurate estimation of the dispersion parameter and in turn calculation of significance for the fold-changes. Also, the moving average of the fold-change was calculated by ordering the genes included in the DESeq2 dataset by length and then calculating the median of a window of 300 genes around these gene. No moving average was calculated for the 75 longest and shortest genes as they did not have an even number of genes on either site for moving average calculation. Furthermore, gene lists of up- or downregulated genes were used for metagenome analysis with ngs.plot (Shen et al, 2014).

For the ChIP-seq dataset, cohesin peaks were called using MACS2 (Zhang et al, 2008b). The files generated were then imported into R, where they were annotated using the package ChIPpeakAnno (Zhu et al, 2010) with gene lists downloaded using the biomaRt package (Durinck et al, 2009). The lists of genes overlapping or with their gene end closest to the peak middle with cohesin peaks were read into ngs.plot (Shen et al, 2014) for metagenome analysis. After analysis had been performed, the data were replotted using the internal R plotting.

Gene set enrichment analysis (GSEA) was performed using the Broad Institute software (http://www.broad.mit.edu/gsea) (Subramanian et al, 2005) using *S. cerevisiae* gene sets from the Xijin Ge lab (http://ge-lab.org/#/data) (Lai et al, 2016).

The GSEA enrichment map was created using the EnrichmentMap plugin (Merico et al, 2010) for Cytoscape (Shannon et al, 2003), broadly following a published protocol (Reimand et al, 2019). Groupings were facilitated by the Cytoscape AutoAnnotate plugin (Kucera et al, 2016). In the comparison of WT vs. *rad30Δ* cells, only gene sets enriched with an adjusted *p*-value of < 0.05 were plotted. In the comparison of both WT and *rad30Δ* cells ± DSB induction, only gene sets enriched with an adjusted *p*-value of < 0.05 and a normalized enrichment score (NES) > 2 for either strain were plotted.

Statistical significance of the overlapping genes in the Venn diagrams was calculated using either a normal approximation or the hypergeometric probability formula. The online tool on http://nemates.org/MA/progs/overlap_stats.html was used for evaluation.

Damage-induced cohesion assay and controls

All strains used harbor the *smc1* temperature sensitive allele (*smc1-259*). The experiments with the P_{GAL}-*HO* allele for DSB induction were performed as described (Wu et al, 2020). The experimental design is also illustrated in Appendix Fig2. In assays utilizing γ-irradiation as DSB source, exponentially growing cells were treated with benomyl (80 µg/ml) in YEPR (raffinose, final 2%) at 23°C for G_2/M arrest. Galactose (final 2%) was then added for one hour to induce expression of the ectopic P_{GAL}-*SMC1-MYC*. The culture was subsequently pelleted and resuspended in 1X PBS, supplemented with benomyl. Half of the resuspension was exposed to γ-irradiation (250 Gy), half was used as non-irradiated control. After irradiation the cells were allowed to recover in YEPG (galactose, final 2%) for one hour, before raising

the temperature to the restrictive 35°C. Samples were then collected during 90 minutes. Damage-induced cohesion was monitored with the Tet-operators/ Tet-repressor-GFP ("Tet-O/TetR-GFP") system. Proper G_2/M arrest, expression of the ectopic Smc1-Myc and DSBs induction were confirmed with FACS analysis, Western blot, and pulsed-field gel electrophoresis (PFGE) respectively (Wu et al, 2020). Efficiency of γ-irradiation was analyzed with Southern blot after PFGE, with a probe for chromosome XVI, as described (Sjogren & Nasmyth, 2001). Analysis of damage-induced cohesion in the *htz1Δ* mutant is described in the appendix supplementary methods.

MNase digestion assay

G_2/M arrested cells were crosslinked *in vivo* with formaldehyde (final 0.5%), for 20 minutes at 23°C. To quench the reaction, glycine (final 125 mM) was added in cultures for 10 minutes. The cells were then harvested and stored at -80°C. Prior to MNase digestion, the cells were resuspended in pre-incubation solution (final 20 mM citric acid, 20 mM Na_2HPO_4, 40 mM EDTA, pH 8.0), with aliquots taken for cell-counting. The final volume of resuspension was subsequently adjusted to have 4.5 x 10^7 cells/ml. The cells were pre-treated with freshly added 2-mercaptoethanol (2-ME, final 30 mM in pre-incubation buffer) for 10 minutes at 30°C, followed by zymolyase treatment in zymolyase buffer (final 1 M sorbitol, 50 mM Tris-HCl (pH 7.5), 10 mM 2-ME and 1 mg/ml 100T zymolyase) for 30-35 minutes (Lantermann et al, 2009). Converted spheroplasts were washed once with cold zymolyase buffer without 2-ME, resuspended in nystatin buffer (final 50 mM NaCl, 1.5 mM $CaCl_2$, 20 mM Tris-HCl

(pH 8.0), 1 M sorbitol, and 100 ug/ml nystatin (Sigma), and then kept on ice temporarily.

The following MNase digestion was performed for each strain individually. Resuspended spheroplasts were sequentially added into the MNase aliquots (ranged from final 0.0125 to 0.1 U/ml, prepared in nystatin buffer), and incubated at 25°C for 15 minutes. Reactions were stopped by adding 1% SDS/12 mM EDTA (final concentration) (Celona et al, 2011; Venditti & Camilloni, 1994). Subsequently, the spheroplasts were treated with RNase (final 0.02 µg/µl) at 37°C for 45 minutes, followed by proteinase K (final 0.4 µg/µl) at 65°C, overnight. The DNA samples were purified with phenol/chloroform extraction, precipitated with ethanol overnight and then resuspended in 1X TE. The samples (2.5 µg) were analyzed with gel electrophoresis (1.2% TAE agarose gel, at 35 V overnight) (Lantermann et al, 2009).

Acknowledgements

We thank K. Shirahige and Y. Katou for support and technical assistance during collection of the previously published ChIP-Seq data. We thank C. Björkegren for sharing strains and plasmids, and for critical reading of the manuscript. This work was supported by the Swedish Research Council (2016-02206), the Swedish Cancer Society (2016/554, 2019/410), the Bergvall Foundation (2016-01868, 2017-02287) and the Karolinska Institutet PhD student financing program (3-1818/2013) to L. Ström. L. Baranello was supported by the Swedish Cancer Society (2018/760), the Karolinska Institutet PhD student financing program (2-5586/2017) and Knut and Alice Wallenberg foundation (2016.0161).

Author contributions

P-S W and LS conceived the study. P-S W designed and performed the experiments, supervised by LS. DC and JG analyzed and prepared figures for the RNA-sequencing and ChIP-sequencing data, supervised by LB. P-S W analyzed the rest of data and prepared figures. P-S W wrote the original draft, P-S W and LS revised and edited the manuscript with input from all authors.

Conflict of interest

The authors declare that they have no conflict of interest.

Data availability

The datasets and computer code related to this study are available in the following databases:

- RNA-seq data: Gene Expression Omnibus 163287 (https//www.ncbi.nlm.nih.gov/geo/query/acc.cgi?acc=GSE163287)
- ChIP-seq data: Gene Expression Omnibus 42655 (https://www.ncbi.nlm.nih.gov/geo/query/acc.cgi?acc=GSE42655)

References

Acharya N, Manohar K, Peroumal D, Khandagale P, Patel SK, Sahu SR, Kumari P (2019) Multifaceted activities of DNA polymerase eta: beyond translesion DNA synthesis. *Current genetics* **65:** 649-656

Bausch C, Noone S, Henry JM, Gaudenz K, Sanderson B, Seidel C, Gerton JL (2007) Transcription alters chromosomal locations of cohesin in Saccharomyces cerevisiae. *Molecular and cellular biology* **27:** 8522-8532

Bhardwaj S, Schlackow M, Rabajdova M, Gullerova M (2016) Transcription facilitates sister chromatid cohesion on chromosomal arms. *Nucleic acids research* **44:** 6676-6692

Bi X, Yu Q, Siler J, Li C, Khan A (2015) Functions of Fun30 chromatin remodeler in regulating cellular resistance to genotoxic stress. *PloS one* **10:** e0121341

Biswas D, Dutta-Biswas R, Mitra D, Shibata Y, Strahl BD, Formosa T, Stillman DJ (2006) Opposing roles for Set2 and yFACT in regulating TBP binding at promoters. *The EMBO journal* **25:** 4479-4489

Celona B, Weiner A, Di Felice F, Mancuso FM, Cesarini E, Rossi RL, Gregory L, Baban D, Rossetti G, Grianti P, Pagani M, Bonaldi T, Ragoussis J, Friedman N, Camilloni G, Bianchi ME, Agresti A (2011) Substantial histone reduction modulates genomewide nucleosomal occupancy and global transcriptional output. *PLoS biology* **9:** e1001086

Ciosk R, Shirayama M, Shevchenko A, Tanaka T, Toth A, Shevchenko A, Nasmyth K (2000) Cohesin's binding to chromosomes depends on a separate complex consisting of Scc2 and Scc4 proteins. *Molecular cell* **5:** 243-254

Costigan C, Kolodrubetz D, Snyder M (1994) NHP6A and NHP6B, which encode HMG1-like proteins, are candidates for downstream components of the yeast SLT2 mitogen-activated protein kinase pathway. *Molecular and cellular biology* **14:** 2391-2403

Davidson IF, Bauer B, Goetz D, Tang W, Wutz G, Peters JM (2019) DNA loop extrusion by human cohesin. *Science* **366:** 1338-1345

Desmoucelles C, Pinson B, Saint-Marc C, Daignan-Fornier B (2002) Screening the yeast "disruptome" for mutants affecting resistance to the immunosuppressive drug, mycophenolic acid. *The Journal of biological chemistry* **277:** 27036-27044

Dion MF, Kaplan T, Kim M, Buratowski S, Friedman N, Rando OJ (2007) Dynamics of replication-independent histone turnover in budding yeast. *Science* **315:** 1405-1408

Dion V, Kalck V, Horigome C, Towbin BD, Gasser SM (2012) Increased mobility of double-strand breaks requires Mec1, Rad9 and the homologous recombination machinery. *Nature cell biology* **14:** 502-509

Dion V, Kalck V, Seeber A, Schleker T, Gasser SM (2013) Cohesin and the nucleolus constrain the mobility of spontaneous repair foci. *EMBO reports* **14:** 984-991

Dorsett D, Strom L (2012) The ancient and evolving roles of cohesin in gene expression and DNA repair. *Current biology : CB* **22:** R240-250

Durinck S, Spellman PT, Birney E, Huber W (2009) Mapping identifiers for the integration of genomic datasets with the R/Bioconductor package biomaRt. *Nature protocols* **4:** 1184-1191

Enervald E, Lindgren E, Katou Y, Shirahige K, Strom L (2013) Importance of Poleta for damage-induced cohesion reveals differential regulation of cohesion establishment at the break site and genome-wide. *PLoS genetics* **9:** e1003158

Formosa T, Eriksson P, Wittmeyer J, Ginn J, Yu Y, Stillman DJ (2001) Spt16-Pob3 and the HMG protein Nhp6 combine to form the nucleosome-binding factor SPN. *The EMBO journal* **20:** 3506-3517

Galdieri L, Zhang T, Rogerson D, Vancura A (2016) Reduced Histone Expression or a Defect in Chromatin Assembly Induces Respiration. *Molecular and cellular biology* **36:** 1064-1077

Gali VK, Balint E, Serbyn N, Frittmann O, Stutz F, Unk I (2017) Translesion synthesis DNA polymerase eta exhibits a specific RNA extension activity and a transcription-associated function. *Scientific reports* **7:** 13055

Garcia-Luis J, Lazar-Stefanita L, Gutierrez-Escribano P, Thierry A, Cournac A, Garcia A, Gonzalez S, Sanchez M, Jarmuz A, Montoya A, Dore M, Kramer H, Karimi MM, Antequera F, Koszul R, Aragon L (2019) FACT mediates cohesin function on chromatin. *Nature structural & molecular biology* **26:** 970-979

Gossett AJ, Lieb JD (2012) In vivo effects of histone H3 depletion on nucleosome occupancy and position in Saccharomyces cerevisiae. *PLoS genetics* **8:** e1002771

Govind CK, Qiu H, Ginsburg DS, Ruan C, Hofmeyer K, Hu C, Swaminathan V, Workman JL, Li B, Hinnebusch AG (2010) Phosphorylated Pol II CTD recruits multiple HDACs, including Rpd3C(S), for methylation-dependent deacetylation of ORF nucleosomes. *Molecular cell* **39:** 234-246

Green EM, Antczak AJ, Bailey AO, Franco AA, Wu KJ, Yates JR, 3rd, Kaufman PD (2005) Replication-independent histone deposition by the HIR complex and Asf1. *Current biology : CB* **15:** 2044-2049

Haarhuis JHI, van der Weide RH, Blomen VA, Yanez-Cuna JO, Amendola M, van Ruiten MS, Krijger PHL, Teunissen H, Medema RH, van Steensel B, Brummelkamp TR, de Wit E, Rowland BD (2017) The Cohesin Release Factor WAPL Restricts Chromatin Loop Extension. *Cell* **169:** 693-707 e614

Hepp MI, Alarcon V, Dutta A, Workman JL, Gutierrez JL (2014) Nucleosome remodeling by the SWI/SNF complex is enhanced by yeast high mobility group box (HMGB) proteins. *Biochimica et biophysica acta* **1839:** 764-772

Hsieh TH, Weiner A, Lajoie B, Dekker J, Friedman N, Rando OJ (2015) Mapping Nucleosome Resolution Chromosome Folding in Yeast by Micro-C. *Cell* **162:** 108-119

Johnson RE, Prakash S, Prakash L (1999) Efficient bypass of a thymine-thymine dimer by yeast DNA polymerase, Poleta. *Science* **283:** 1001-1004

Joshi RS, Pina B, Roca J (2012) Topoisomerase II is required for the production of long Pol II gene transcripts in yeast. *Nucleic acids research* **40:** 7907-7915

Kaufman PD, Cohen JL, Osley MA (1998) Hir proteins are required for position-dependent gene silencing in Saccharomyces cerevisiae in the absence of chromatin assembly factor I. *Molecular and cellular biology* **18:** 4793-4806

Kim D, Paggi JM, Park C, Bennett C, Salzberg SL (2019a) Graph-based genome alignment and genotyping with HISAT2 and HISAT-genotype. *Nature biotechnology* **37:** 907-915

Kim Y, Shi Z, Zhang H, Finkelstein IJ, Yu H (2019b) Human cohesin compacts DNA by loop extrusion. *Science* **366:** 1345-1349

Kizer KO, Phatnani HP, Shibata Y, Hall H, Greenleaf AL, Strahl BD (2005) A novel domain in Set2 mediates RNA polymerase II interaction and couples histone H3 K36 methylation with transcript elongation. *Molecular and cellular biology* **25:** 3305-3316

Kozlova AL, Valieva ME, Maluchenko NV, Studitsky VM (2018) HMGB Proteins as DNA Chaperones That Modulate Chromatin Activity. *Molekuliarnaia biologiia* **52:** 737-749

Krogan NJ, Baetz K, Keogh MC, Datta N, Sawa C, Kwok TC, Thompson NJ, Davey MG, Pootoolal J, Hughes TR, Emili A, Buratowski S, Hieter P, Greenblatt JF (2004) Regulation of chromosome stability by the histone H2A variant Htz1, the Swr1 chromatin remodeling complex, and the histone acetyltransferase NuA4. *Proceedings of the National Academy of Sciences of the United States of America* **101:** 13513-13518

Kucera M, Isserlin R, Arkhangorodsky A, Bader GD (2016) AutoAnnotate: A Cytoscape app for summarizing networks with semantic annotations. *F1000Research* **5:** 1717

Kushnirov VV (2000) Rapid and reliable protein extraction from yeast. *Yeast* **16:** 857-860

Lai L, Hennessey J, Bares V, Son EW, Ban Y, Wang W, Qi J, Jiang G, Liberzon A, Xijin Ge S (2016) GSKB: A gene set database for pathway analysis in mouse. *bioRxiv***:** 082511

Landry J, Sutton A, Hesman T, Min J, Xu RM, Johnston M, Sternglanz R (2003) Set2-catalyzed methylation of histone H3 represses basal expression of GAL4 in Saccharomyces cerevisiae. *Molecular and cellular biology* **23:** 5972-5978

Langmead B, Trapnell C, Pop M, Salzberg SL (2009) Ultrafast and memory-efficient alignment of short DNA sequences to the human genome. *Genome biology* **10:** R25

Lantermann A, Stralfors A, Fagerstrom-Billai F, Korber P, Ekwall K (2009) Genome-wide mapping of nucleosome positions in Schizosaccharomyces pombe. *Methods* **48:** 218-225

Lazar-Stefanita L, Scolari VF, Mercy G, Muller H, Guerin TM, Thierry A, Mozziconacci J, Koszul R (2017) Cohesins and condensins orchestrate the 4D dynamics of yeast chromosomes during the cell cycle. *The EMBO journal* **36:** 2684-2697

Lengronne A, Katou Y, Mori S, Yokobayashi S, Kelly GP, Itoh T, Watanabe Y, Shirahige K, Uhlmann F (2004) Cohesin relocation from sites of chromosomal loading to places of convergent transcription. *Nature* **430:** 573-578

Lengronne A, McIntyre J, Katou Y, Kanoh Y, Hopfner KP, Shirahige K, Uhlmann F (2006) Establishment of sister chromatid cohesion at the S. cerevisiae replication fork. *Molecular cell* **23:** 787-799

Li B, Pattenden SG, Lee D, Gutierrez J, Chen J, Seidel C, Gerton J, Workman JL (2005) Preferential occupancy of histone variant H2AZ at inactive promoters influences local histone modifications and chromatin remodeling. *Proceedings of the National Academy of Sciences of the United States of America* **102:** 18385-18390

Li H, Durbin R (2009) Fast and accurate short read alignment with Burrows-Wheeler transform. *Bioinformatics* **25:** 1754-1760

Liao Y, Smyth GK, Shi W (2014) featureCounts: an efficient general purpose program for assigning sequence reads to genomic features. *Bioinformatics* **30:** 923-930

Lopez-Serra L, Kelly G, Patel H, Stewart A, Uhlmann F (2014) The Scc2-Scc4 complex acts in sister chromatid cohesion and transcriptional regulation by maintaining nucleosome-free regions. *Nature genetics* **46:** 1147-1151

Love MI, Huber W, Anders S (2014) Moderated estimation of fold change and dispersion for RNA-seq data with DESeq2. *Genome biology* **15:** 550

Lyons NA, Fonslow BR, Diedrich JK, Yates JR, 3rd, Morgan DO (2013) Sequential primed kinases create a damage-responsive phosphodegron on Eco1. *Nature structural & molecular biology* **20:** 194-201

Lyons NA, Morgan DO (2011) Cdk1-dependent destruction of Eco1 prevents cohesion establishment after S phase. *Molecular cell* **42:** 378-389

Martin M (2011) Cutadapt removes adapter sequences from high-throughput sequencing reads. *2011* **17:** 3

McCarthy DJ, Chen Y, Smyth GK (2012) Differential expression analysis of multifactor RNA-Seq experiments with respect to biological variation. *Nucleic acids research* **40:** 4288-4297

McKay BC, Stubbert LJ, Fowler CC, Smith JM, Cardamore RA, Spronck JC (2004) Regulation of ultraviolet light-induced gene expression by gene size. *Proceedings of the National Academy of Sciences of the United States of America* **101:** 6582-6586

Merico D, Isserlin R, Stueker O, Emili A, Bader GD (2010) Enrichment map: a network-based method for gene-set enrichment visualization and interpretation. *PloS one* **5:** e13984

Mine-Hattab J, Rothstein R (2012) Increased chromosome mobility facilitates homology search during recombination. *Nature cell biology* **14:** 510-517

Morillo-Huesca M, Clemente-Ruiz M, Andujar E, Prado F (2010) The SWR1 histone replacement complex causes genetic instability and genome-wide transcription misregulation in the absence of H2A.Z. *PloS one* **5:** e12143

Paull TT, Carey M, Johnson RC (1996) Yeast HMG proteins NHP6A/B potentiate promoter-specific transcriptional activation in vivo and assembly of preinitiation complexes in vitro. *Genes & development* **10:** 2769-2781

Paull TT, Johnson RC (1995) DNA looping by Saccharomyces cerevisiae high mobility group proteins NHP6A/B. Consequences for nucleoprotein complex assembly and chromatin condensation. *The Journal of biological chemistry* **270:** 8744-8754

Prochasson P, Florens L, Swanson SK, Washburn MP, Workman JL (2005) The HIR corepressor complex binds to nucleosomes generating a distinct protein/DNA complex resistant to remodeling by SWI/SNF. *Genes & development* **19:** 2534-2539

Ramirez F, Ryan DP, Gruning B, Bhardwaj V, Kilpert F, Richter AS, Heyne S, Dundar F, Manke T (2016) deepTools2: a next generation web server for deep-sequencing data analysis. *Nucleic acids research* **44:** W160-165

Reimand J, Isserlin R, Voisin V, Kucera M, Tannus-Lopes C, Rostamianfar A, Wadi L, Meyer M, Wong J, Xu C, Merico D, Bader GD (2019) Pathway enrichment analysis and visualization of omics data using g:Profiler, GSEA, Cytoscape and EnrichmentMap. *Nature protocols* **14:** 482-517

Rhee HS, Bataille AR, Zhang L, Pugh BF (2014) Subnucleosomal structures and nucleosome asymmetry across a genome. *Cell* **159:** 1377-1388

Rhoades AR, Ruone S, Formosa T (2004) Structural features of nucleosomes reorganized by yeast FACT and its HMG box component, Nhp6. *Molecular and cellular biology* **24:** 3907-3917

Robinson MD, McCarthy DJ, Smyth GK (2010) edgeR: a Bioconductor package for differential expression analysis of digital gene expression data. *Bioinformatics* **26:** 139-140

Rolef Ben-Shahar T, Heeger S, Lehane C, East P, Flynn H, Skehel M, Uhlmann F (2008) Eco1-dependent cohesin acetylation during establishment of sister chromatid cohesion. *Science* **321:** 563-566

Ruan C, Lee CH, Cui H, Li S, Li B (2015) Nucleosome contact triggers conformational changes of Rpd3S driving high-affinity H3K36me nucleosome engagement. *Cell reports* **10:** 204-215

Rufiange A, Jacques PE, Bhat W, Robert F, Nourani A (2007) Genome-wide replication-independent histone H3 exchange occurs predominantly at promoters and implicates H3 K56 acetylation and Asf1. *Molecular cell* **27:** 393-405

Sagot I, Schaeffer J, Daignan-Fornier B (2005) Guanylic nucleotide starvation affects Saccharomyces cerevisiae mother-daughter separation and may be a signal for entry into quiescence. *BMC cell biology* **6:** 24

Schalbetter SA, Goloborodko A, Fudenberg G, Belton JM, Miles C, Yu M, Dekker J, Mirny L, Baxter J (2017) SMC complexes differentially compact mitotic chromosomes according to genomic context. *Nature cell biology* **19:** 1071-1080

Segovia R, Shen Y, Lujan SA, Jones SJ, Stirling PC (2017) Hypermutation signature reveals a slippage and realignment model of translesion synthesis by Rev3 polymerase in cisplatin-treated yeast. *Proceedings of the National Academy of Sciences of the United States of America* **114:** 2663-2668

Shannon P, Markiel A, Ozier O, Baliga NS, Wang JT, Ramage D, Amin N, Schwikowski B, Ideker T (2003) Cytoscape: a software environment for integrated models of biomolecular interaction networks. *Genome research* **13:** 2498-2504

Sharma U, Stefanova D, Holmes SG (2013) Histone variant H2A.Z functions in sister chromatid cohesion in Saccharomyces cerevisiae. *Molecular and cellular biology* **33:** 3473-3481

Sharp JA, Franco AA, Osley MA, Kaufman PD (2002) Chromatin assembly factor I and Hir proteins contribute to building functional kinetochores in S. cerevisiae. *Genes & development* **16:** 85-100

Shen L, Shao N, Liu X, Nestler E (2014) ngs.plot: Quick mining and visualization of next-generation sequencing data by integrating genomic databases. *BMC genomics* **15:** 284

Sherwood PW, Tsang SV, Osley MA (1993) Characterization of HIR1 and HIR2, two genes required for regulation of histone gene transcription in Saccharomyces cerevisiae. *Molecular and cellular biology* **13:** 28-38

Sjogren C, Nasmyth K (2001) Sister chromatid cohesion is required for postreplicative double-strand break repair in Saccharomyces cerevisiae. *Current biology : CB* **11:** 991-995

Srinivasan M, Fumasoni M, Petela NJ, Murray A, Nasmyth KA (2020) Cohesion is established during DNA replication utilising chromosome associated cohesin rings as well as those loaded de novo onto nascent DNAs. *eLife* **9**

Strahl BD, Grant PA, Briggs SD, Sun ZW, Bone JR, Caldwell JA, Mollah S, Cook RG, Shabanowitz J, Hunt DF, Allis CD (2002) Set2 is a nucleosomal histone H3-selective methyltransferase that mediates transcriptional repression. *Molecular and cellular biology* **22:** 1298-1306

Strom L, Karlsson C, Lindroos HB, Wedahl S, Katou Y, Shirahige K, Sjogren C (2007) Postreplicative formation of cohesion is required for repair and induced by a single DNA break. *Science* **317:** 242-245

Strom L, Lindroos HB, Shirahige K, Sjogren C (2004) Postreplicative recruitment of cohesin to double-strand breaks is required for DNA repair. *Molecular cell* **16:** 1003-1015

Subramanian A, Tamayo P, Mootha VK, Mukherjee S, Ebert BL, Gillette MA, Paulovich A, Pomeroy SL, Golub TR, Lander ES, Mesirov JP (2005) Gene set enrichment analysis: a knowledge-based approach for interpreting genome-wide expression profiles. *Proceedings of the National Academy of Sciences of the United States of America* **102:** 15545-15550

Szerlong H, Saha A, Cairns BR (2003) The nuclear actin-related proteins Arp7 and Arp9: a dimeric module that cooperates with architectural proteins for chromatin remodeling. *The EMBO journal* **22:** 3175-3187

Terweij M, van Leeuwen F (2013) Histone exchange: sculpting the epigenome. *Frontiers in Life Science* **7:** 63-79

Trask DK, Muller MT (1988) Stabilization of type I topoisomerase-DNA covalent complexes by actinomycin D. *Proceedings of the National Academy of Sciences of the United States of America* **85:** 1417-1421

Uhlmann F, Lottspeich F, Nasmyth K (1999) Sister-chromatid separation at anaphase onset is promoted by cleavage of the cohesin subunit Scc1. *Nature* **400:** 37-42

Unal E, Heidinger-Pauli JM, Kim W, Guacci V, Onn I, Gygi SP, Koshland DE (2008) A molecular determinant for the establishment of sister chromatid cohesion. *Science* **321:** 566-569

Unal E, Heidinger-Pauli JM, Koshland D (2007) DNA double-strand breaks trigger genome-wide sister-chromatid cohesion through Eco1 (Ctf7). *Science* **317:** 245-248

van Steensel B, Furlong EEM (2019) The role of transcription in shaping the spatial organization of the genome. *Nature reviews Molecular cell biology* **20:** 327-337

Venditti S, Camilloni G (1994) In vivo analysis of chromatin following nystatin-mediated import of active enzymes into Saccharomyces cerevisiae. *Molecular & general genetics : MGG* **242:** 100-104

Venkatesh S, Smolle M, Li H, Gogol MM, Saint M, Kumar S, Natarajan K, Workman JL (2012) Set2 methylation of histone H3 lysine 36 suppresses histone exchange on transcribed genes. *Nature* **489:** 452-455

Venkatesh S, Workman JL (2015) Histone exchange, chromatin structure and the regulation of transcription. *Nature reviews Molecular cell biology* **16:** 178-189

Weber CM, Ramachandran S, Henikoff S (2014) Nucleosomes are context-specific, H2A.Z-modulated barriers to RNA polymerase. *Molecular cell* **53:** 819-830

Williamson L, Saponaro M, Boeing S, East P, Mitter R, Kantidakis T, Kelly GP, Lobley A, Walker J, Spencer-Dene B, Howell M, Stewart A, Svejstrup JQ (2017) UV Irradiation Induces a Non-coding RNA that Functionally Opposes the Protein Encoded by the Same Gene. *Cell* **168:** 843-855 e813

Wu PS, Enervald E, Joelsson A, Palmberg C, Rutishauser D, Hallberg BM, Strom L (2020) Posttranslational Regulation of DNA Polymerase eta, a Connection to Damage-Induced Cohesion in Saccharomyces cerevisiae. *Genetics* **216:** 1009-1022

Xin H, Takahata S, Blanksma M, McCullough L, Stillman DJ, Formosa T (2009) yFACT induces global accessibility of nucleosomal DNA without H2A-H2B displacement. *Molecular cell* **35:** 365-376

Yen YM, Wong B, Johnson RC (1998) Determinants of DNA binding and bending by the Saccharomyces cerevisiae high mobility group protein NHP6A that are important for its biological activities. Role of the unique N terminus and putative intercalating methionine. *The Journal of biological chemistry* **273:** 4424-4435

Yu R, Sun L, Sun Y, Han X, Qin L, Dang W (2019) Cellular response to moderate chromatin architectural defects promotes longevity. *Science advances* **5:** eaav1165

Yu Y, Eriksson P, Stillman DJ (2000) Architectural transcription factors and the SAGA complex function in parallel pathways to activate transcription. *Molecular and cellular biology* **20:** 2350-2357

Zhang H, Roberts DN, Cairns BR (2005) Genome-wide dynamics of Htz1, a histone H2A variant that poises repressed/basal promoters for activation through histone loss. *Cell* **123:** 219-231

Zhang J, Shi D, Li X, Ding L, Tang J, Liu C, Shirahige K, Cao Q, Lou H (2017) Rtt101-Mms1-Mms22 coordinates replication-coupled sister chromatid cohesion and nucleosome assembly. *EMBO reports* **18:** 1294-1305

Zhang J, Shi X, Li Y, Kim BJ, Jia J, Huang Z, Yang T, Fu X, Jung SY, Wang Y, Zhang P, Kim ST, Pan X, Qin J (2008a) Acetylation of Smc3 by Eco1 is required for S phase sister chromatid cohesion in both human and yeast. *Molecular cell* **31:** 143-151

Zhang Y, Liu T, Meyer CA, Eeckhoute J, Johnson DS, Bernstein BE, Nusbaum C, Myers RM, Brown M, Li W, Liu XS (2008b) Model-based analysis of ChIP-Seq (MACS). *Genome biology* **9:** R137

Zhu LJ, Gazin C, Lawson ND, Pages H, Lin SM, Lapointe DS, Green MR (2010) ChIPpeakAnno: a Bioconductor package to annotate ChIP-seq and ChIP-chip data. *BMC bioinformatics* **11:** 237

Main figure legends

Figure 1. A potential role for Polη in facilitating chromatin association of RNAPII

A. Spot assay to monitor sensitivity of the *rad30Δ* mutant to the transcription elongation inhibitors, actinomycin D and mycophenolic acid (MPA). Tenfold serial dilutions of indicated mid-log phase cells on the controls (-Ura plate ± guanine), and the drug-containing plates, after 3-day incubation.

B. ChIP-qPCR analyses to determine chromatin association of Rpb1 in indicated strains, on selected actively transcribed genes in G_2/M arrested WT cells. Error bars indicate the mean ± STDEV of two independent experiments. Asterisks denote significant differences compared to the WT cells at indicated position ($p < 0.05$; One-way ANOVA, Tukey post hoc test). p, promoter; m, mid; e, end of gene body. n1 and n2, non-binding controls.

C-D. Western blot analysis of Rpb1 stability. G_2/M arrested cells from indicated strains, with or without one-hour P_{GAL}-*HO* break induction, were pelleted and resuspended in media containing cycloheximide (CHX) to monitor Rpb1 protein level without further protein synthesis. Cdc11 was used as loading control. M, protein marker.

Figure 2. Transcription is perturbed in *rad30Δ* mutants

A-C. Volcano plots showing differentially expressed genes between WT and *rad30Δ* cells, before and after DSB, determined by RNA-seq. Each dot represents one gene.

Red and blue dots represent up- and down-regulated genes respectively. Numbers of differentially expressed genes are indicated. Black dots indicate that expression of these genes was not significantly changed (< $-Log_{10}(0.5)$). *p*adj, adjusted *p* value.

D-E. Comparisons between expression level of genes significantly up (D) or downregulated (E) in the WT+DSB relative to the G_2/M arrested WT cells, and expression of the same set of genes in the *rad30Δ* mutant, based on RNA-seq analysis.

F. Plot of fold change moving median, sorted by length (300 genes/window) to monitor the trend of gene expression after DSB in relation to gene length, comparing WT and *rad30Δ* cells. Fold change values were based on the changes of gene expression in WT and *rad30Δ* cells after DSB, determined by RNA-seq.

Figure 3. Increased cohesin binding around TSS in *rad30Δ* cells

A. Metagenome plot showing cohesin enrichment ± 1000 bp from the transcription start site (TSS) in WT and *rad30Δ* cells ± DSB induction in G_2/M phase. The samples were first normalized to their respective input and then the values were scaled to the maximum value of the plot.

B. The data from (A) plotted relative to the WT-DSB sample. After normalizing to the input, all samples were also normalized to WT-DSB sample to visualize the changes between the WT and *rad30Δ* cells.

C. Metagenome plot showing cohesin distribution 1000 bp downstream and 100 bp upstream from the transcription end site (TES) in WT and *rad30Δ* cells ± DSB induction in G_2/M phase. Plotted as in (A).

D. As in (B), except plotting cohesin distribution around the TES according to (C).

Figure 4. Genes involved in chromatin assembly and positive transcription regulation pathways are downregulated in the absence of Polη

A. Relatively enriched pathways in G_2/M arrested WT and *rad30Δ* cells, plotted with Cytoscape after gene set enrichment analysis (GSEA). The GSEA was performed with gene lists ranked by $\log_{10} p$ value (multiplied by the sign of the fold change) of each gene. The number of genes in each gene set is proportional to the circle size. Lines connect gene sets with similarity greater than 0.7. All gene sets have FDR < 0.05.

B. Gene set enrichment analysis after DSB induction, plotted with Cytoscape to depict the difference between WT and *rad30Δ* cells in up- or down-regulation of indicated pathways after DSB. Gene expression of WT and *rad30Δ* cells after DSB was compared to that of respective G_2/M arrested cells. GSEA was performed as in A. The lines indicate the same as in A. All gene sets have FDR < 0.05 and a normalized enrichment score > 2 for at least one of the WT or *rad30Δ* cells.

Figure 5. Histone exchange at promoters affects formation of damage-induced cohesion

A. Damage-induced cohesion assays of the *hir1Δ* single and *hir1Δrad30Δ* double mutants after P_{GAL}-*HO* induction, performed as illustrated in Appendix Fig 2A. Means ± STDEV from at least two independent experiments are shown.

B. Damage-induced cohesion assay of the *htz1Δ* mutant after γ-irradiation, performed according to the procedure described in the Appendix supplementary methods. Means ± STDEV from at least two independent experiments are shown.

Figure 6. Globally reduced nucleosome occupancy does not affect formation of damage-induced cohesion

A. Damage-induced cohesion assay of the *nhp6aΔnhp6bΔ* mutant after γ-irradiation, performed as illustrated in Appendix Fig 2B. Means ± STDEV from at least two independent experiments are shown.

B-C. Damage-induced cohesion assays of the *hhf1-hht1Δ* and *hht2-hhf2Δ* mutants after P_{GAL}-*HO* induction, performed as illustrated in Appendix Fig 2A. Means ± STDEV from at least two independent experiments are shown.

Figure 7. A positive role of Polη in transcription is essential for generation of damage-induced cohesion

A. Spot assay to monitor the effect of *SET2* deletion on the *rad30Δ* mutant sensitivity to the transcription elongation inhibitors, actinomycin D and mycophenolic acid (MPA). Tenfold serial dilutions of indicated mid-log phase cells on control (-Ura plate ± guanine) and drug-containing plates, after 3-day incubation.

B. Damage-induced cohesion assay of the *set2Δ* mutant after P_{GAL}-*HO* induction, performed as depicted in Appendix Fig 2A. Means ± STDEV from at least two independent experiments are shown.

C. A simplified illustration summarizing the main results from this study. In G_2/M arrested WT cells, genes belonging to the positive transcription regulation and chromatin assembly pathways are enriched compared to *rad30*Δ cells. Reduced chromatin assembly in *rad30*Δ cells results in less dynamic chromatin, indicated by additional nucleosomes. Deregulated transcription and sensitivity to elongation inhibitors in *rad30*Δ cells are indicated by thin arrows over the TSS and ORF. Histone exchange between H3 and H3K56Ac at promoter regions is reduced in the *hir1*Δ mutant, thereby affecting transcription negatively. Histone exchange of H2A for H2A.Z at the +1 nucleosome is prevented in the *htz1Δ* mutant, whereby transcription is hampered and/or deregulated. Both mutants were deficient in damage-induced cohesion. Nucleosome occupancy is reduced at the +1 nucleosome but increased within ORFs in the *nhp6aΔnhp6bΔ* mutant. Regulation of transcription elongation is altered in the *set2Δ* mutant. In both cases transcription is promoted, and both mutants suppressed the lack of damage-induced cohesion in *rad30Δ* cells. Cells with a single green dot indicates established damage-induced cohesion while cells with two dots indicates lack of damage-induced cohesion. ORF, open reading frame.

Expanded view figure legends

Figure EV1. Results connected to Figure 2 and 3

A. FACS analysis to confirm benomyl-induced G_2/M arrest. 1G, 1-hour *GAL*-induction (P_{GAL}-*HO*).

B. PFGE analysis to monitor DSB induction on chromosome III. G2, G_2/M arrest; 1G as in A.

C. PCA to demonstrate distribution of independent data sets between groups and clustering of data sets within groups.

D. Venn diagrams showing overlaps of differentially expressed genes in WT and *rad30Δ* cells after DSB, based on RNA-seq. The red and blue arrows indicate up- and down-regulated genes respectively. Statistical significance of the overlapping genes was evaluated as described in Materials and Methods, with * $p < 0.001$.

E. Expression changes of short genes (< 500 bp) after DSB in WT and *rad30Δ* cells. Genes with or without cohesin enrichment were defined according to the Scc1 ChIP-seq data.

Figure EV2. Results connected to Figure 4

A. Monitoring activation of DNA damage checkpoint (phosphorylation of Rad53) after DSB induction with western blot. Galactose was added into the G_2/M arrested cell cultures to induce P_{GAL}-*HO* break induction for 1- or 1.5-hour, denoted as 1G or 1.5G. Sample collected from G_2/M arrested WT cells, treated with phleomycin (final 15 μg/ml) for 1.5 hours was included as positive control (PC). Cdc11 was used as loading control. M, protein marker.

B. Monitoring activation of DNA damage checkpoint during DSB recovery. DSB was induced for 1- or 1.5-hour, as in A. The cells were then allowed to recover in YEP media supplemented with glucose and benomyl for another 1.5 hour (1.5 R) at 35°C,

to mimic the damage-induced cohesion assay. 1G, 1.5G, PC, M as in A. Cdc11 was used as loading control.

C. FACS analyses of cell cycle progression in WT and *rad30Δ* cells, at indicated time points after release into YEP media supplemented with glucose after DSB induction. Samples without DSBs were included as control. B, benomyl; R, recovery.

Figure EV3. Control experiments connected to Figure 5

A. FACS analysis to confirm G_2/M arrest during the time course of a typical damage-induced cohesion assay. 3B, 3-hour benomyl arrest.

B. PFGE analysis to detect DSB induction on chromosome III. 1, G_2/M arrest; 2, 1-hour *GAL*-induction (P_{GAL}-*HO* and P_{GAL}-*SMC1-MYC*).

C. Western blot to check expression of the *GAL* promoter driven ectopic Smc1-Myc protein. G2, G_2/M arrest; 1G, 1-hour *GAL*-induction as in B. Cdc11 was used as loading control. M, protein marker.

D. Damage-induced cohesion assay of the *hir1Δ* mutant in response to γ-irradiation, performed as depicted in Appendix Fig 2B. Means ± STDEV from at least two independent experiments are shown.

E. Sister chromatid cohesion maintenance of the *htz1Δ* mutant under prolonged G_2/M arrest. The cells were initially synchronized in G_1 by α-factor in YEP media containing galactose. Expression of P_{GAL}-*CDC20* was then shut off by switching the carbon source to glucose (YEPD), which resulted in the subsequent prolonged G_2/M arrest as monitored by FACS (left panel). Sister chromatid separation was monitored at the *URA3* locus on Chr. V by the TetO/TetR-GFP system. Means ± STDEV from at least

two independent experiments are shown (right panel). A *rad61Δ* mutant with known high sister separation under prolonged G_2/M arrest was included as control. Means ± STDEV from at least two independent experiments are shown. Parts of the results from the same experiments were previously published (Wu et al, 2020). Chr., chromosome.

Figure EV4. Control experiments connected to Figure 6

A. Sister chromatid separation in non-irradiated samples, used as negative control for the damage-induced cohesion assay in Fig 6A. S-phase cohesion was inactivated at 35°C, the restrictive temperature for the *smc1-259 ts* allele. Means ± STDEV from at least two independent experiments are shown.

B. Reduced chromatin accessibility of the G_2/M arrested *nhp6aΔnhp6bΔ* mutant. The concentration of MNase was ranged from 0, 0.0125, 0.025, 0.05, 0.1 U/ml (final). One representative gel electrophoresis result from at least two independent assays performed is shown. M, DNA ladder; Un, undigested; 1x, monomer; 2x, dimer; 3x, trimer; 4x, tetramer.

Appendix figure legends

Appendix Figure 1. Quantitation of Rpb1 levels

A-B. Relative amount of Rpb1 after addition of water (A, control) or galactose (B) to induce P_{GAL}-*HO* DSB induction for one-hour, followed by cycloheximide (CHX) chase up to 150 minutes. Western blots from two independent experiments were quantified to compare Rpb1 levels (relative to Cdc11) between the indicated strains.

Appendix Figure 2. Methods to monitor damage-induced cohesion

A. Damage-induced cohesion assay performed with *GAL* induced DSBs on chromosome III (P_{GAL}-*HO*). Strains harboring the temperature sensitive *smc1-259* allele are arrested in G_2/M by addition of benomyl (B). Galactose is then added for expression of ectopic P_{GAL}-*SMC1-MYC* (Smc1 WT) and induction of DSBs, for 1-hour. The temperature is then raised to 35°C, restrictive to the *smc1-259* allele, for disruption of S-phase cohesion (blue rings). The Tet-O/TetR-GFP system (green dots) is used to monitor damage-induced cohesion (red rings) on chr. V. Chr., chromosome; III, three; V, five. B1 and 2 indicates replacement of media with freshly prepared benomyl.

B. Damage-induced cohesion assay performed with γ-irradiation. Formation of damage-induced cohesion is monitored on chr. V with the same Tet-O/TetR-GFP system, as in A, with slight differences in the experimental procedure. Strains with *smc1-259* background are arrested in G_2/M by addition of benomyl (B), expression of ectopic P_{GAL}-*SMC1-MYC* (Smc1 WT) is then induced by addition of galactose. The cells are subsequently pelleted, resuspended in 1X PBS supplemented with

benomyl. The resuspension is split in one half for irradiation, and half as non-irradiated control. After irradiation, both ± irradiated cells are recovering in YEP media supplemented with galactose and benomyl. Subsequently, the media is changed to YEP containing glucose and benomyl, and the temperature raised to 35°C, to monitor formation of damage-induced cohesion.

Appendix supplementary methods

Damage-induced cohesion assay for the *htz1Δ* mutant

Considering that the *htz1Δ* mutant is benomyl sensitive (Krogan et al, 2004), the strains used in this assay contain the P_{MET}-*CDC20* and *smc1-259 ts* alleles. The strains were grown in methionine drop-out media (-Met) to log phase at 23°C. To arrest cells in G_2/M phase, expression of *CDC20* was repressed by replacing the media to YEP supplemented with Met (final 2 mM) and 0.1% glucose. Galactose (final 2%) was then added for 1.5 hours to induce expression of ectopic Smc1-Myc, driven by the *GAL* promoter. The cultures were subsequently split into half and resuspended in 1X PBS. One half for γ-irradiation (250 Gy), and another half as non-irradiated control. After 1-hour recovery in YEP media supplemented with galactose and Met, the temperature was raised to 35°C and damage-induced cohesion was monitored for 90 min.

Appendix Table 1. Primary antibody information

Antibody	Company	Catalog #
anti-Rpb1 (8WG16)	Santa Cruz Biotechnology	sc-56767
anti-Cdc11 (y-415)	Santa Cruz Biotechnology	sc-7170
anti-Rad53	Abcam	ab104232
anti-c-myc	Roche	11667203001

Fig 1

A

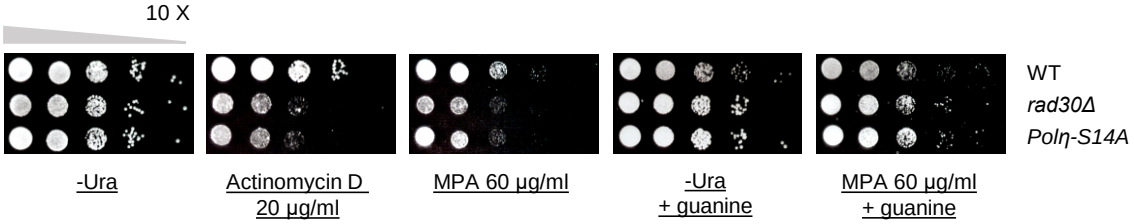

B

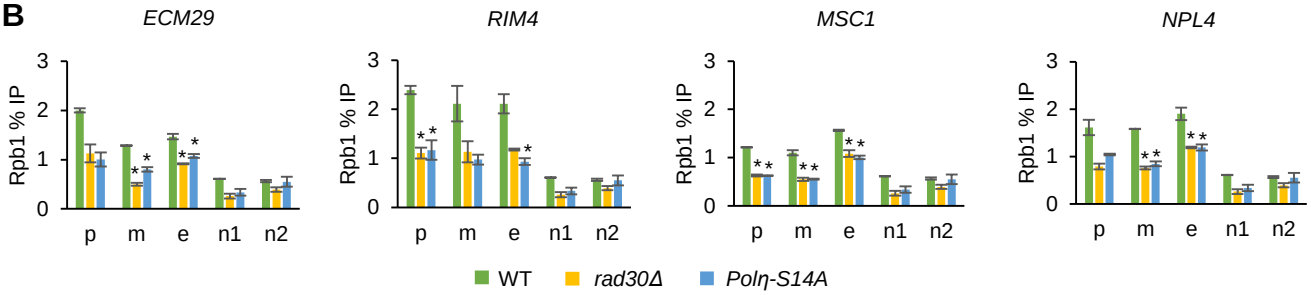

C G_2/M - P_{GAL}-*HO*

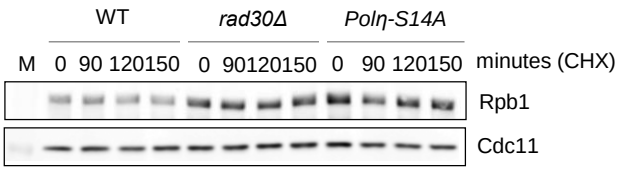

D G_2/M + P_{GAL}-*HO*

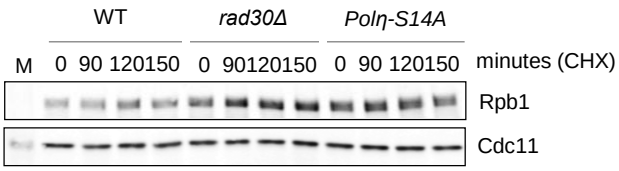

Fig 2

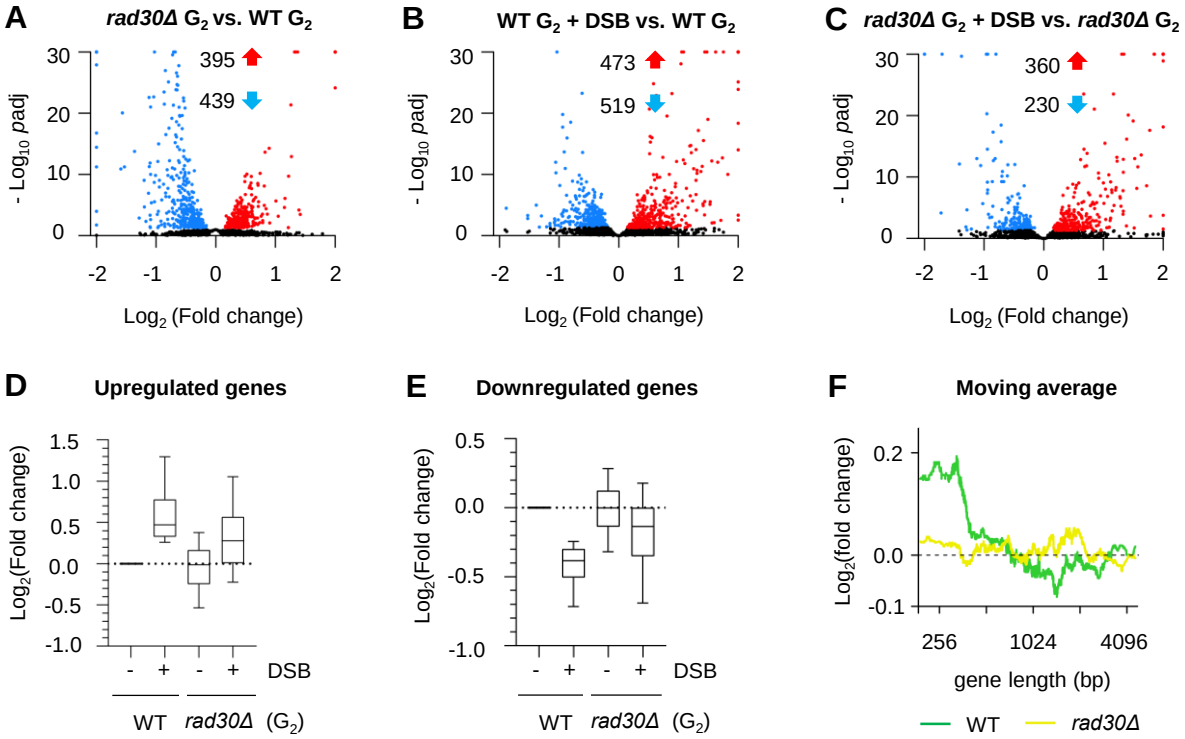
A
rad30Δ G2 vs. WT G2
395
439
- Log10 padj
Log2 (Fold change)
B
WT G2 + DSB vs. WT G2
473
519
- Log10 padj
Log2 (Fold change)
C
rad30Δ G2 + DSB vs. rad30Δ G2
360
230
- Log10 padj
Log2 (Fold change)
D
Upregulated genes
Log2(Fold change)
DSB
WT
rad30Δ
(G2)
E
Downregulated genes
Log2(Fold change)
DSB
WT
rad30Δ
(G2)
F
Moving average
Log2(fold change)
gene length (bp)
WT
rad30Δ

Fig 3

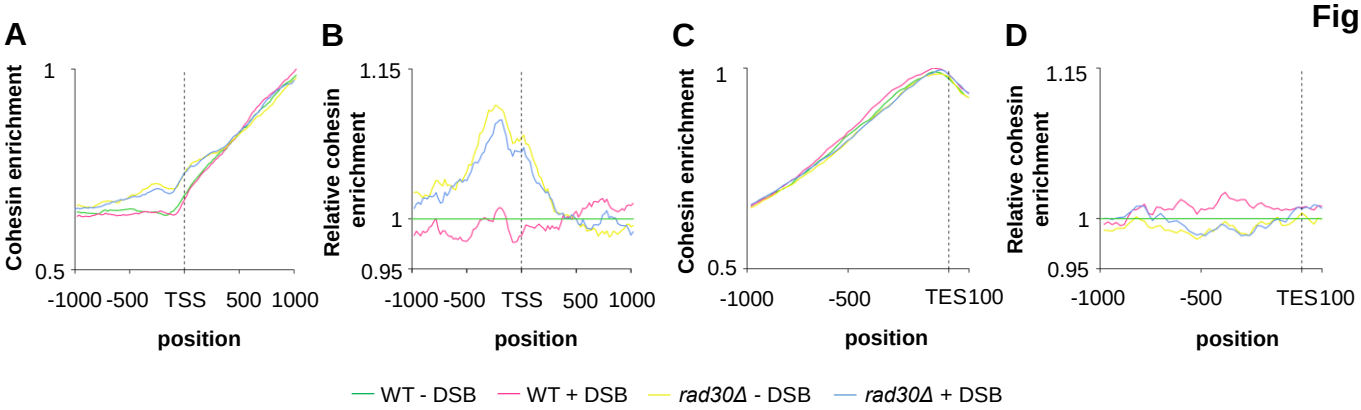
A
Cohesin enrichment
1
0.5
-1000 -500 TSS 500 1000
position
B
Relative cohesin enrichment
1.15
1
0.95
-1000 -500 TSS 500 1000
position
C
Cohesin enrichment
1
0.5
-1000 -500 TES 100
position
D
Relative cohesin enrichment
1.15
1
0.95
-1000 -500 TES 100
position
WT - DSB
WT + DSB
rad30Δ - DSB
rad30Δ + DSB

Fig 4

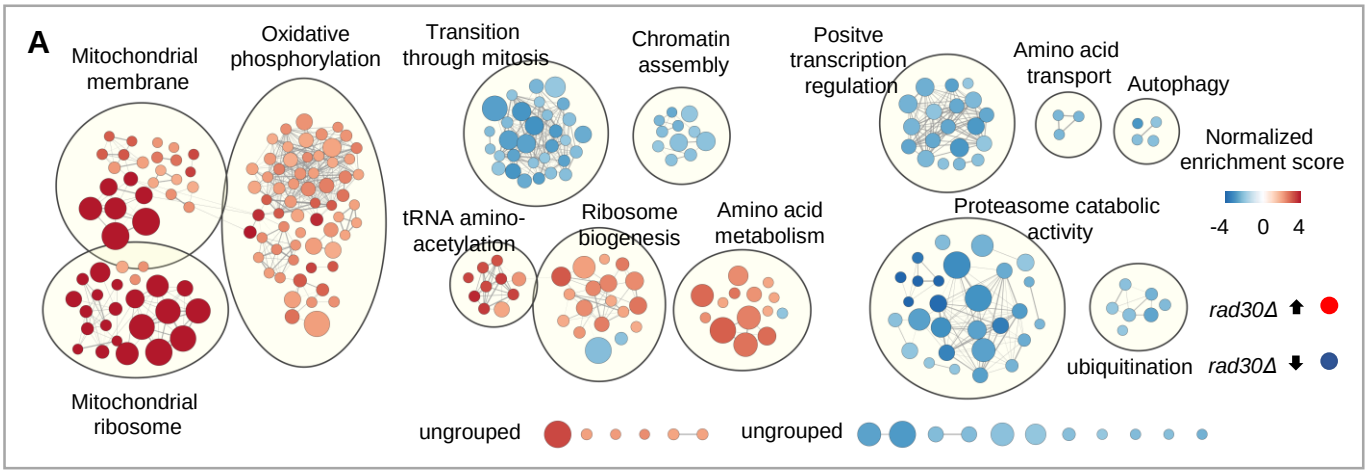
A
Mitochondrial membrane
Oxidative phosphorylation
Transition through mitosis
Chromatin assembly
Positve transcription regulation
Amino acid transport
Autophagy
Normalized enrichment score
-4 0 4
tRNA amino-acetylation
Ribosome biogenesis
Amino acid metabolism
Proteasome catabolic activity
ubiquitination
rad30Δ
rad30Δ
Mitochondrial ribosome
ungrouped
ungrouped

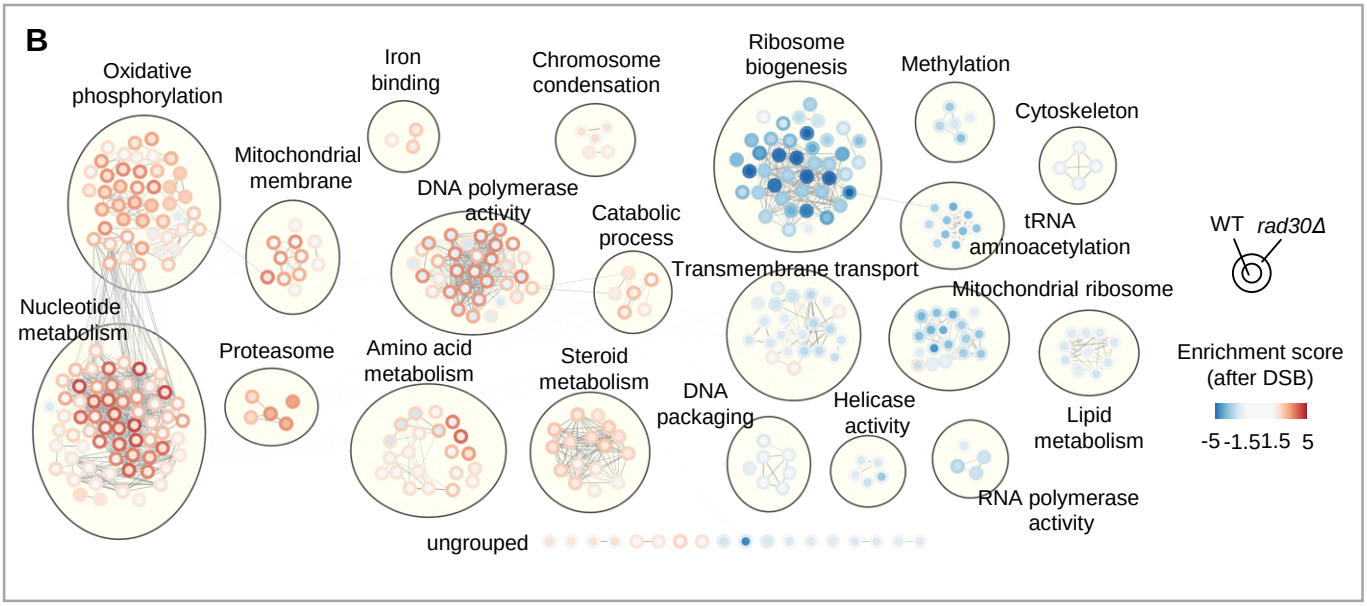
B
Oxidative phosphorylation
Iron binding
Chromosome condensation
Ribosome biogenesis
Methylation
Cytoskeleton
Mitochondrial membrane
DNA polymerase activity
Catabolic process
tRNA aminoacetylation
Transmembrane transport
Mitochondrial ribosome
WT
rad30Δ
Nucleotide metabolism
Proteasome
Amino acid metabolism
Steroid metabolism
DNA packaging
Helicase activity
Lipid metabolism
Enrichment score (after DSB)
-5 -1.5 1.5 5
RNA polymerase activity
ungrouped

Fig 5

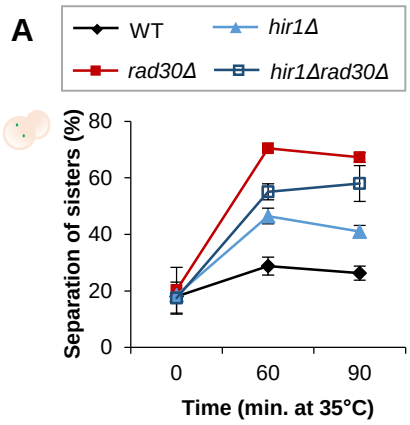
A
WT
hir1Δ
rad30Δ
hir1Δrad30Δ
Separation of sisters (%)
80
60
40
20
0
0
60
90
Time (min. at 35°C)

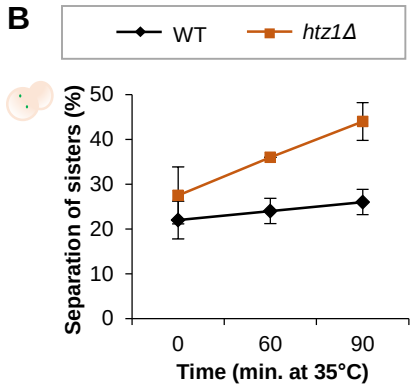
B
WT
htz1Δ
Separation of sisters (%)
50
40
30
20
10
0
0
60
90
Time (min. at 35°C)

Fig 6

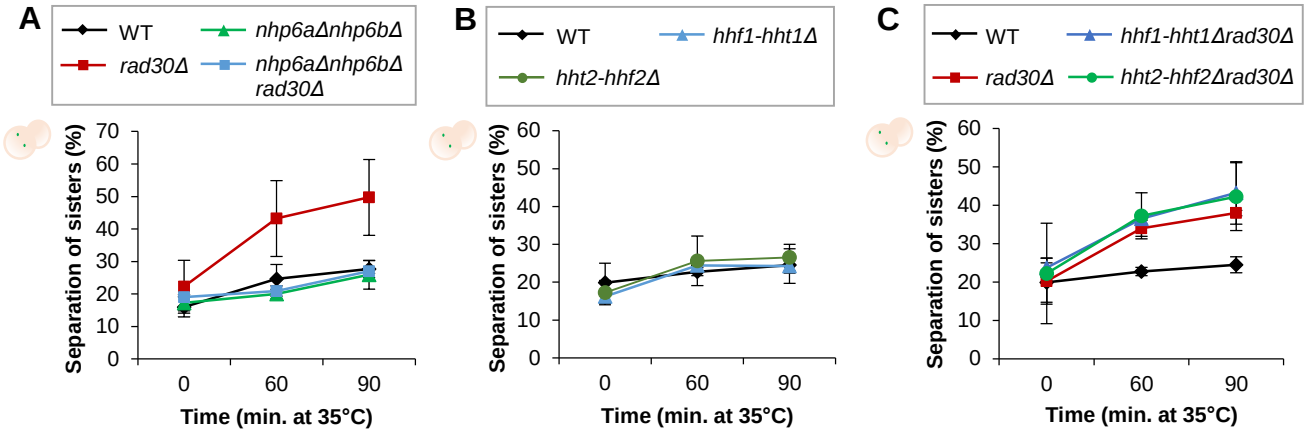
A
WT
nhp6aΔnhp6bΔ
rad30Δ
nhp6aΔnhp6bΔ rad30Δ
Separation of sisters (%)
70
60
50
40
30
20
10
0
0
60
90
Time (min. at 35°C)
B
WT
hhf1-hht1Δ
hht2-hhf2Δ
Separation of sisters (%)
60
50
40
30
20
10
0
0
60
90
Time (min. at 35°C)
C
WT
hhf1-hht1Δrad30Δ
rad30Δ
hht2-hhf2Δrad30Δ
Separation of sisters (%)
60
50
40
30
20
10
0
0
60
90
Time (min. at 35°C)

Fig 7

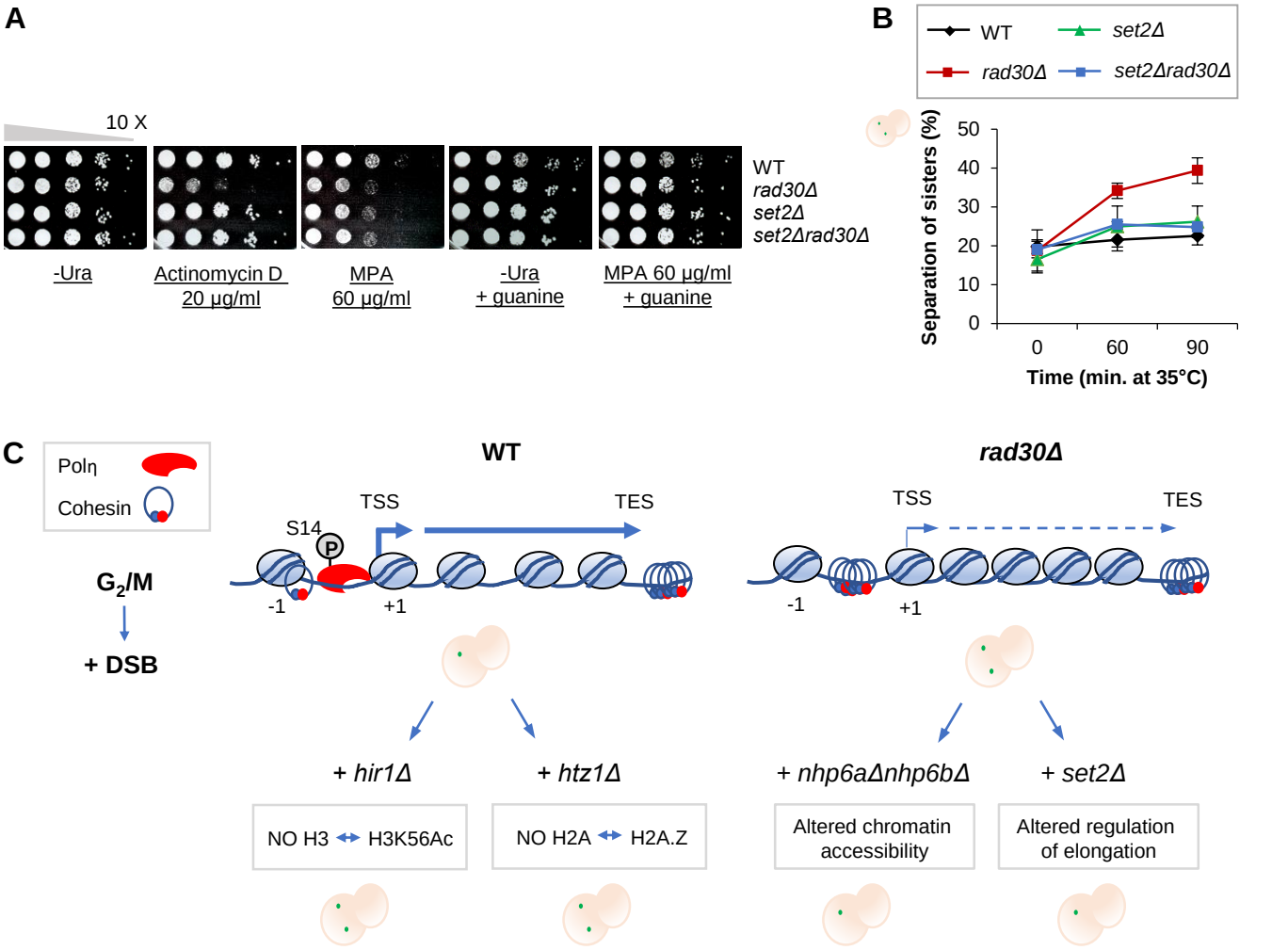
A
10 X
WT
rad30Δ
set2Δ
set2Δrad30Δ
-Ura
Actinomycin D 20 µg/ml
MPA 60 µg/ml
-Ura + guanine
MPA 60 µg/ml + guanine
B
WT
set2Δ
rad30Δ
set2Δrad30Δ
Separation of sisters (%)
50
40
30
20
10
0
0
60
90
Time (min. at 35°C)
C
Polη
Cohesin
G2/M
+ DSB
WT
TSS
TES
S14
P
-1
+1
rad30Δ
TSS
TES
-1
+1
+ hir1Δ
+ htz1Δ
+ nhp6aΔnhp6bΔ
+ set2Δ
NO H3 H3K56Ac
NO H2A H2A.Z
Altered chromatin accessibility
Altered regulation of elongation

Fig EV1

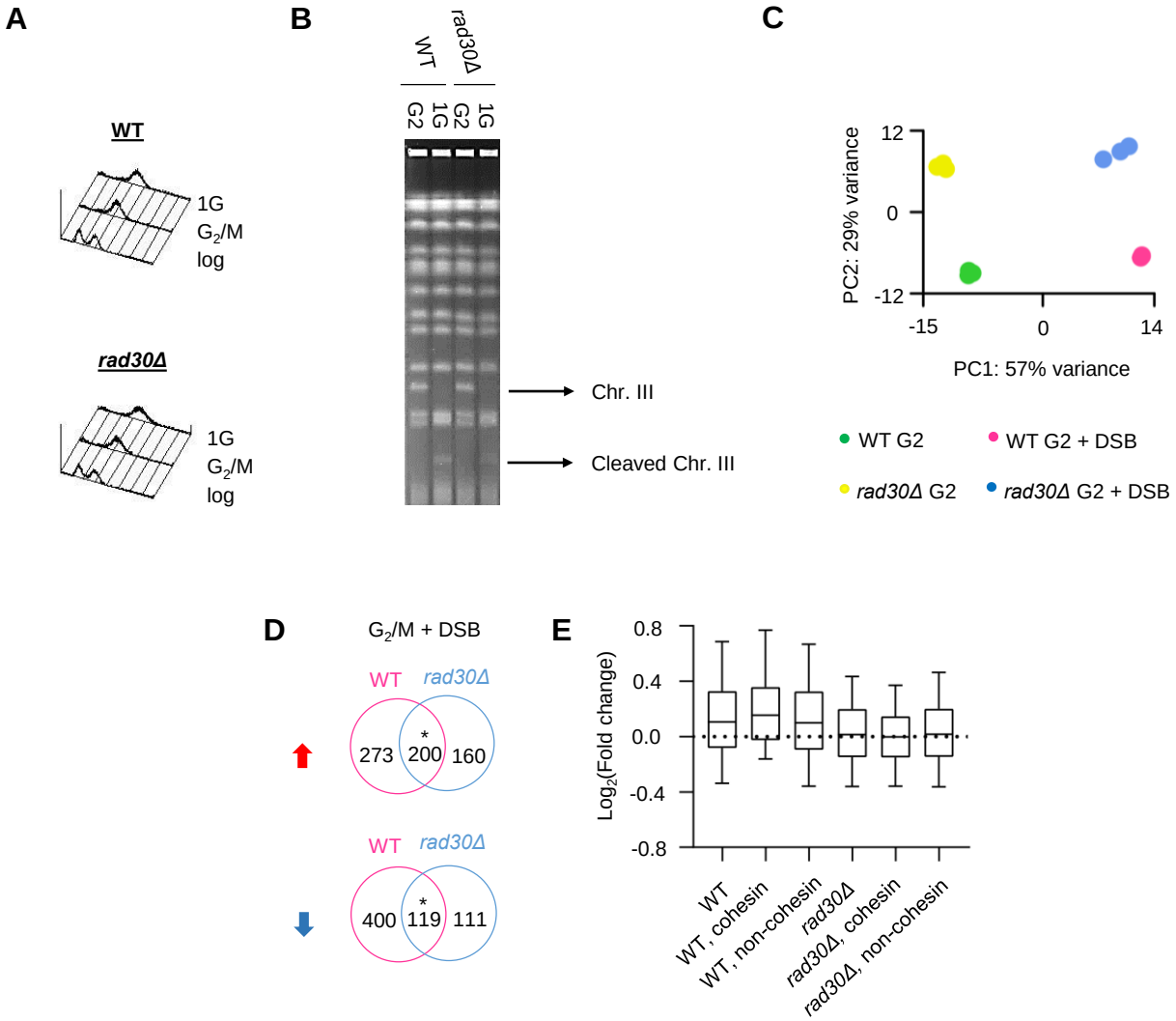
A
WT
1G
G2/M
log
rad30Δ
1G
G2/M
log
B
WT
rad30Δ
G2
1G
G2
1G
Chr. III
Cleaved Chr. III
C
PC2: 29% variance
12
0
-12
-15
0
14
PC1: 57% variance
WT G2
WT G2 + DSB
rad30Δ G2
rad30Δ G2 + DSB
D
G2/M + DSB
WT
rad30Δ
273
*
200
160
WT
rad30Δ
400
*
119
111
E
Log2(Fold change)
0.8
0.4
0.0
-0.4
-0.8
WT
WT, cohesin
WT, non-cohesin
rad30Δ
rad30Δ, cohesin
rad30Δ, non-cohesin

Fig EV2

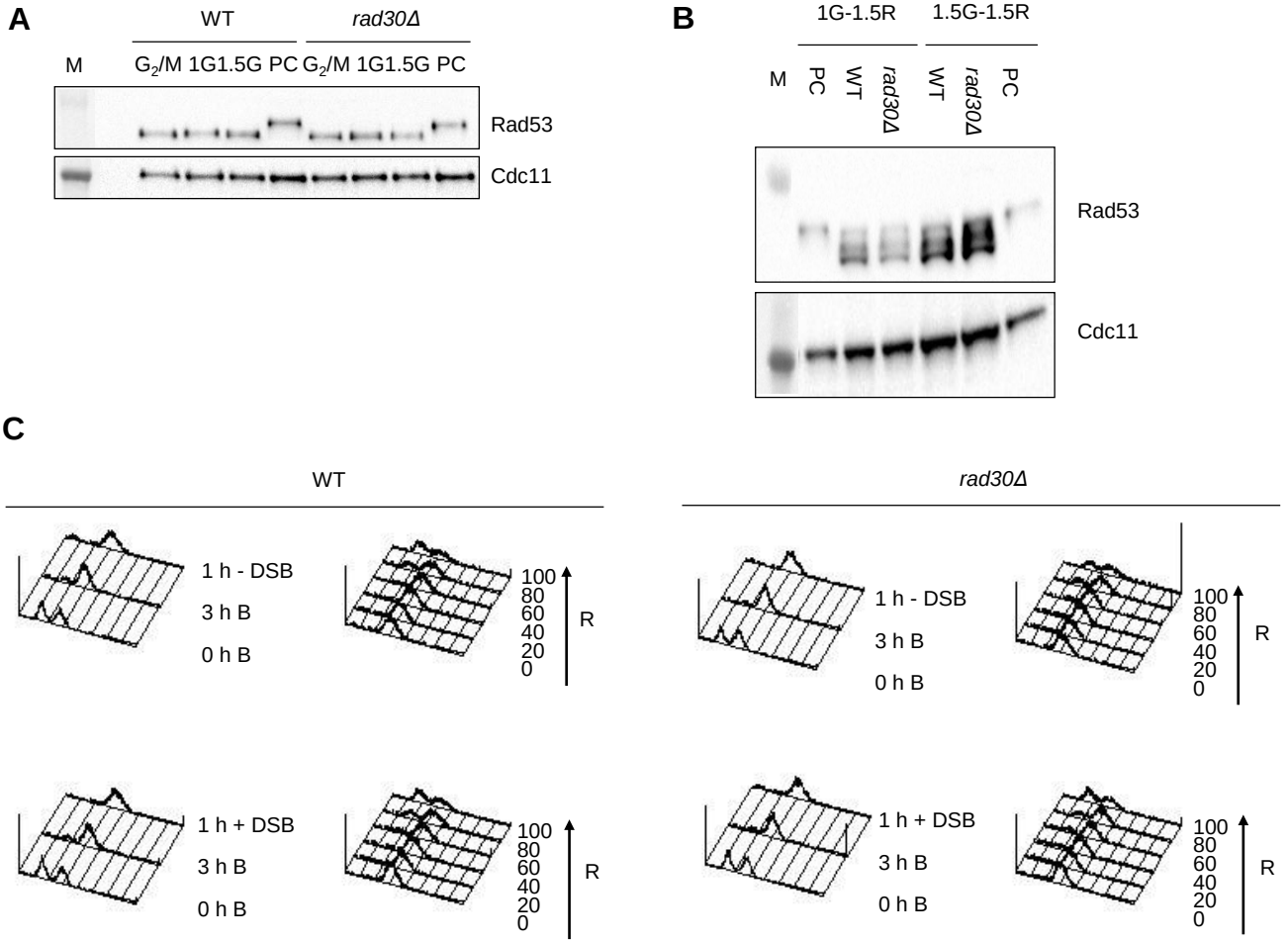
A
WT
rad30Δ
M
G2/M 1G1.5G PC G2/M 1G1.5G PC
Rad53
Cdc11
B
1G-1.5R
1.5G-1.5R
M
PC
WT
rad30Δ
WT
rad30Δ
PC
Rad53
Cdc11
C
WT
rad30Δ
1 h - DSB
3 h B
0 h B
1 h + DSB
3 h B
0 h B
100
80
60
40
20
0
R

Fig EV3

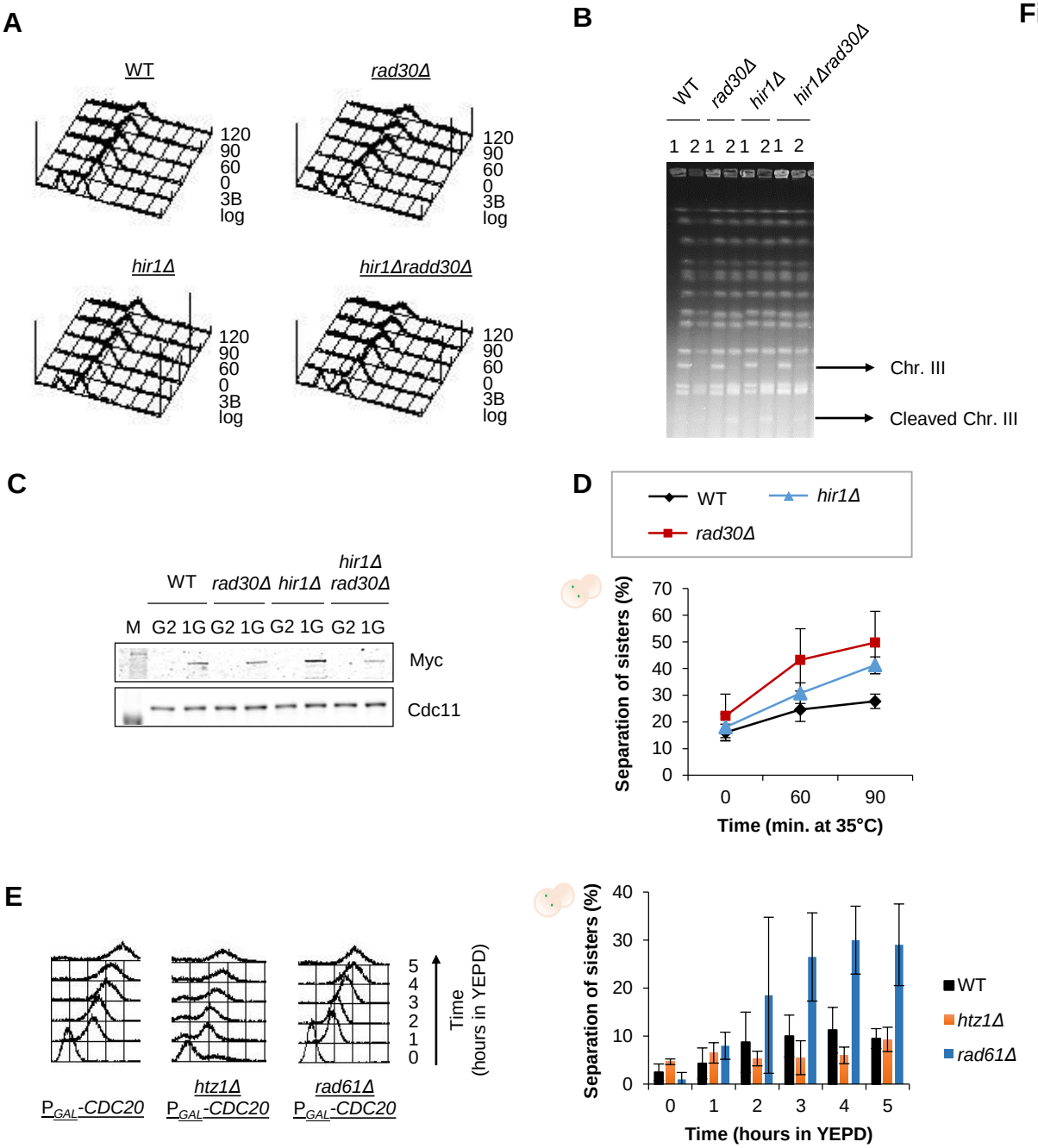
A
WT
rad30Δ
hir1Δ
hir1Δradd30Δ
120
90
60
0
3B
log
B
WT
rad30Δ
hir1Δ
hir1Δrad30Δ
1 2 1 2 1 2 1 2
Chr. III
Cleaved Chr. III
C
WT
rad30Δ
hir1Δ
hir1Δ rad30Δ
M G2 1G G2 1G G2 1G G2 1G
Myc
Cdc11
D
WT
hir1Δ
rad30Δ
Separation of sisters (%)
Time (min. at 35°C)
E
PGAL-CDC20
htz1Δ PGAL-CDC20
rad61Δ PGAL-CDC20
Time (hours in YEPD)
Separation of sisters (%)
Time (hours in YEPD)
WT
htz1Δ
rad61Δ

Fig EV4

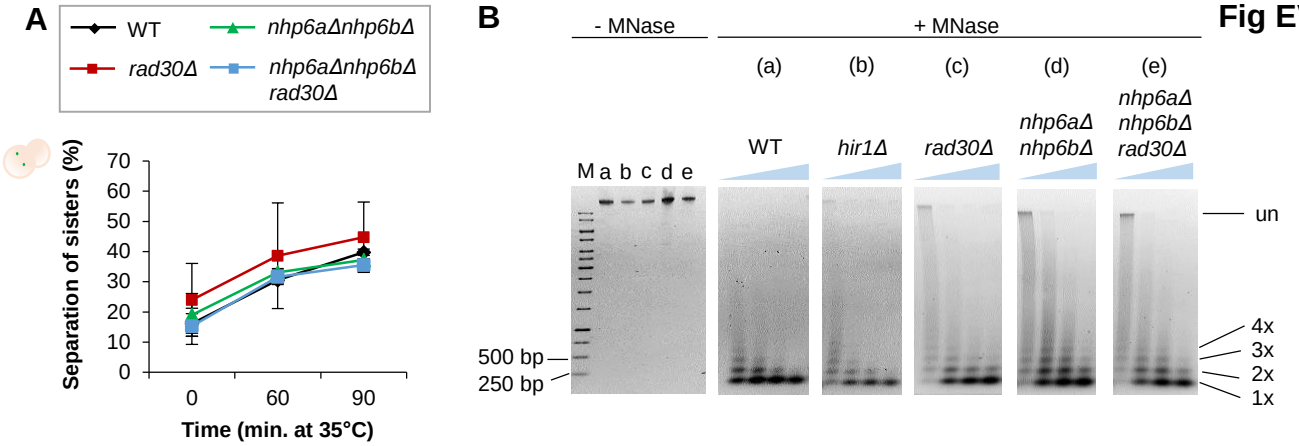
A
WT
nhp6aΔnhp6bΔ
rad30Δ
nhp6aΔnhp6bΔ rad30Δ
Separation of sisters (%)
70
60
50
40
30
20
10
0
0
60
90
Time (min. at 35°C)
B
- MNase
+ MNase
(a)
(b)
(c)
(d)
(e)
WT
hir1Δ
rad30Δ
nhp6aΔ nhp6bΔ
nhp6aΔ nhp6bΔ rad30Δ
M a b c d e
500 bp
250 bp
un
4x
3x
2x
1x

Appendix Fig 1

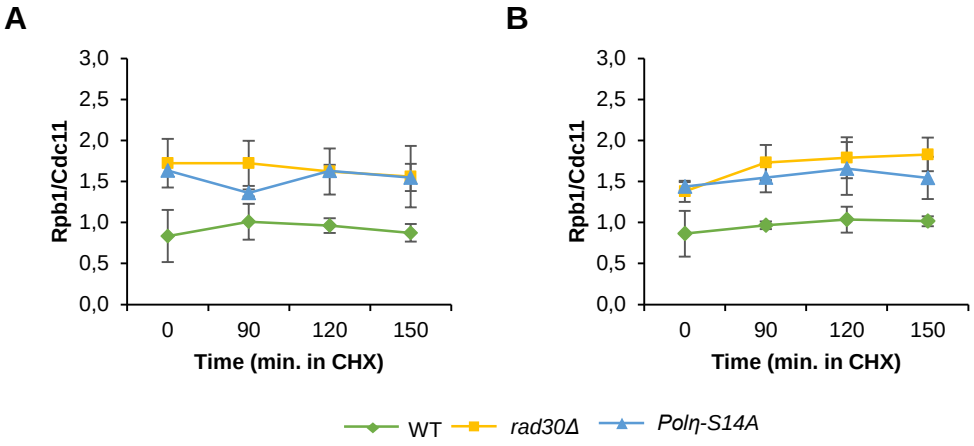

Appendix Fig 2

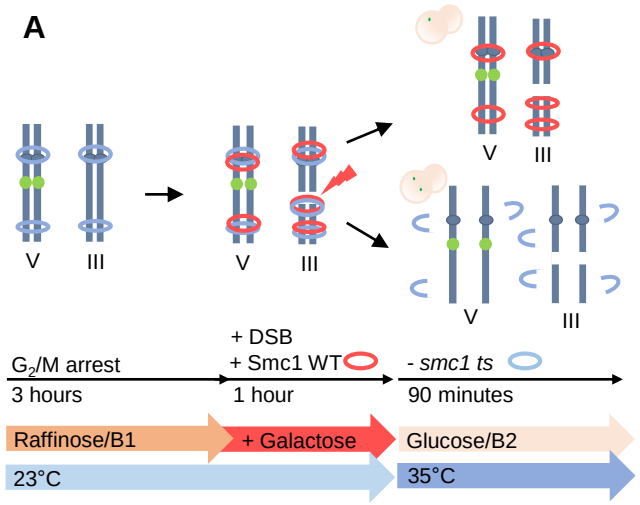

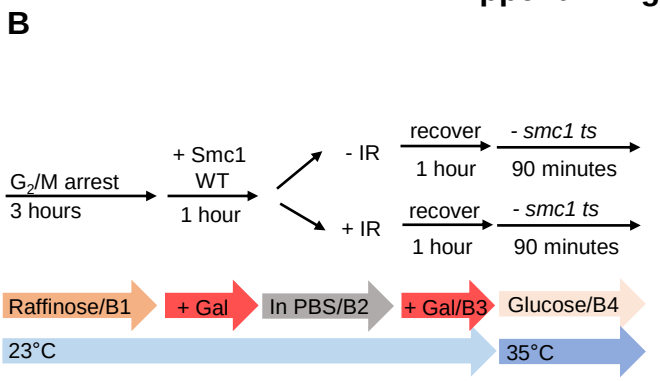

Table EV1. Strains used in this study

Strain (LS)	Genotype
50	*MATa ade3::GALHO ade2-1 trp1-1 can1-100 leu2-3,112 his3-11,15 ura3-1 GAL psi+ RAD5*
421	*MATα rad30::KAN smc1-259 ade3::GALHO leu2-3,112::PGAL-SMC1-MYC-LEU2 his3-11,15::HIS3-tetR-GFP ura3-1::tetOx112-URA3 ade2-1 trp1-1 can1-100 GAL psi+ RAD5*
468	*MATα rad30(S14A)::NAT smc1-259 ade3::GALHO leu2-3,112::PGAL-SMC1-MYC-LEU2 his3-11,15::HIS3-tetR-GFP ura3-1::tetOx112-URA3 ade2-1 trp1-1 can1-100 GAL psi+ RAD5*
514	*MATa rad30::KAN ade3::GALHO ade2-1 trp1-1 can1-100 leu2-3,112 his3-11,15 ura3-1 GAL psi+ RAD5*
655	*MATa smc1-259 ade3::GALHO leu2-3,112::PGAL-SMC1-MYC-LEU2 his3-11,15::HIS3-tetR-GFP ura3-1::tetOx112-URA3 ade2-1 trp1-1 can1-100 GAL psi+ RAD5*
656/1098	MAT*α smc1-259 ade3::GALHO leu2-3,112::PGAL-SMC1-MYC-LEU2 his3-11,15::HIS3-tetR-GFP ura3-1::tetOx112-URA3 ade2-1 trp1-1 can1-100 GAL psi+ RAD5*
657	*MATa smc1-259 leu2-3,112::PGAL-SMC1-MYC-LEU2 his3-11,15::HIS3-tetR-GFP ura3-1::tetOx112-URA3 ade2-1 trp1-1 can1-100 GAL psi+ RAD5*
666	*MATa smc1-259 leu2-3,112::PGAL-SMC1-MYC-LEU2 trp1-1::PMET3-CDC20-TRP1 his3-11,15::HIS3-tetR-GFP ura3-1::tetOx112-URA3 ade2-1 can1-100 GAL psi+ RAD5*
699	*MATa htz1::HPH smc1-259 leu2-3,112::PGAL-SMC1-MYC-LEU2 trp1-1::PMET3-CDC20-TRP1 his3-11,15::HIS3-tetR-GFP ura3-1::tetOx112-URA3 ade2-1 can1-100 GAL psi+ RAD5*
847	*MATa trp1-1::PGAL-CDC20-TRP1(K. lactis) his3-11,15::HIS3-tetR-GFP ura3-1::tetOx112-URA3 ade2-1 can1-100 leu2-3,112 GAL psi+ RAD5*
848	*MATa htz1::HPH trp1-1::PGAL-CDC20-TRP1(K. lactis) his3-11,15::HIS3-tetR-GFP ura3-1::tetOx112-URA3 ade2-1 can1-100 leu2-3,112 GAL psi+ RAD5*
910	*MATa hir1::NAT smc1-259 ade3::GALHO leu2-3,112::PGAL-SMC1-MYC-LEU2 his3-11,15::HIS3-tetR-GFP ura3-1::tetOx112-URA3 ade2-1 trp1-1 can1-100 GAL psi+ RAD5*
914	*MATα hir1::NAT rad30::KAN smc1-259 ade3::GALHO leu2-3,112::PGAL-SMC1-MYC-LEU2 his3-11,15::HIS3-tetR-GFP ura3-1::tetOx112-URA3 ade2-1 trp1-1 can1-100 GAL psi+ RAD5*
928	*MATa rad61::KAN trp1-1::PGAL-CDC20-TRP1(K. lactis) his3-11,15::HIS3-tetR-GFP ura3-1::tetOx112-URA3 ade2-1 can1-100 leu2-3,112 GAL psi+ RAD5*
956	*MATα nhp6a::NAT nhp6b::HPH rad30::KAN smc1-259 leu2-3,112::PGAL-SMC1-MYC-LEU2 his3-11,15::HIS3-tetR-GFP ura3-1::tetOx112-URA3 ade2-1 trp1-1 can1-100 GAL psi+ RAD5*
963	*MATa hir1::HPH smc1-259 leu2-3,112::PGAL-SMC1-MYC-LEU2 his3-11,15::HIS3-tetR-GFP ura3-1::tetOx112-URA3 ade2-1 trp1-1 can1-100 GAL psi+ RAD5*
999	*MATa nhp6a::NAT nhp6b::HPH smc1-259 leu2-3,112::PGAL-SMC1-MYC-LEU2 his3-11,15::HIS3-tetR-GFP ura3-1::tetOx112-URA3 ade2-1 trp1-1 can1-100 GAL psi+ RAD5*
1002	*MATα rad30::KAN smc1-259 leu2-3,112::PGAL-SMC1-MYC-LEU2 his3-11,15::HIS3-tetR-GFP ura3-1::tetOx112-URA3 ade2-1 trp1-1 can1-100 GAL psi+ RAD5*
1054	*MATa hhf1-hht1::HPH smc1-259 ade3::GALHO leu2-3,112::PGAL-SMC1-MYC-LEU2 his3-11,15::HIS3-tetR-GFP ura3-1::tetOx112-URA3 ade2-1 trp1-1 can1-100 GAL psi+ RAD5*
1055	*MATa hht2-hhf2::HPH smc1-259 ade3::GALHO leu2-3,112::PGAL-SMC1-MYC-LEU2 his3-11,15::HIS3-tetR-GFP ura3-1::tetOx112-URA3 ade2-1 trp1-1*

Table EV2. Primers used for Rpb1 ChIP-qPCR

Name	Sequence
ECM29 pro F	TACCAGTTTAGCCGCCAG
ECM29 pro R	CGCAATTCTGCCTTCTCC
ECM29 mid F	ATCGCAGACTCGACTCAC
ECM29 mid R	GTCACTTGGCAGACCAAC
ECM29 end F	ACACATGGAGAACGCAAC
ECM29 end R	CTTCTGAATGATCAGGCCAC
RIM4 pro F	CTCTCTTCCTTTCTCTCTCCC
RIM4 pro R	GAGTCGGCCTTTAGACCATTAG
RIM4 mid F	TGGATCATCGAATGGGCAC
RIM4 mid R	CCTCTGAATCACTACCATGCAC
RIM4 end F	TTATCCCATGTCACCACCTCC
RIM4 end R	GGTACTGCCATGATTAGCAGC
MSC1 pro F	GAGAGGGAGGAAACAAGGAG
MSC1 pro R	CGGAAACCGCATTAACCAAC
MSC1 mid F	CAGAAAAGGCAGAACAGCAG
MSC1 mid R	ACCTTGTGGCTCTCCAAC
MSC1 end F	GGTTGTTCGGCACTGTTAAG
MSC1 end R	GTACATTACGTTGACACCCC
NPL4 pro F	GCCCTCGTAACATACAGAAC
NPL4 pro R	GGTCCAGATTACCCACCAAC
NPL4 mid F	GATATACGAGCCCCCTCAG
NPL4 mid R	CAAAAAACAGACCCATCCCC
NPL4 end F	GCAGATACTCTCTCCAGACG
NPL4 end R	TCTCTCCTAGCCGCTTTC
nonbinding *TAX4* up F (N1)	CCGAAACTGCAAATCCTCC
nonbinding *TAX4* up R (N1)	TTCATCGCTCCTTTCCCC
nonbinding *ADH3* up F (N2)	CACATCCCTTTGAAACGCAC
nonbinding *ADH3* up R (N2)	TACCCTCGACAAATGCCC